2012-06

# Investigation of the Effect of Convergent Detonation on Metal Acceleration and Gurney.

Ludwig, Wibke

NPS-PH-12-001


# NAVAL POSTGRADUATE SCHOOL

**MONTEREY, CALIFORNIA**

**INVESTIGATION OF THE EFFECT OF CONVERGENT DETONATION ON METAL ACCELERATION AND GURNEY**

by

Wibke Ludwig

June 2012

**Approved for public release; distribution is unlimited**

THIS PAGE INTENTIONALLY LEFT BLANK

# REPORT DOCUMENTATION PAGE

*Form Approved*
OMB No. 0704-0188



| **1. REPORT DATE** *(DD-MM-YYYY)* | **2. REPORT TYPE** | **3. DATES COVERED** *(From-To)* |
|---|---|---|
| 13–6–2012 | Technical Report | 02/2012— 06/2012 |

**4. TITLE AND SUBTITLE**

Investigation of the Effect of Convergent Detonation on Metal Acceleration and Gurney

**5a. CONTRACT NUMBER**

**5b. GRANT NUMBER**

**5c. PROGRAM ELEMENT NUMBER**

**6. AUTHOR(S)**

Wibke Ludwig

**5d. PROJECT NUMBER**

**5e. TASK NUMBER**

**5f. WORK UNIT NUMBER**

**7. PERFORMING ORGANIZATION NAME(S) AND ADDRESS(ES) AND ADDRESS(ES)**

Naval Postgraduate School
Monterey, CA 93943

**8. PERFORMING ORGANIZATION REPORT NUMBER**

NPS-PH-12-001

**9. SPONSORING / MONITORING AGENCY NAME(S) AND ADDRESS(ES)**

Helmut-Schmidt-University
University of the Federal Armed Forces Hamburg
Holstenhofweg 85
22043 Hamburg
Germany

**10. SPONSOR/MONITOR'S ACRONYM(S)**

**11. SPONSOR/MONITOR'S REPORT NUMBER(S)**

**12. DISTRIBUTION / AVAILABILITY STATEMENT**

Approved for public release; distribution is unlimited

**13. SUPPLEMENTARY NOTES**

The views expressed in this thesis are those of the author and do not reflect the official policy or position of the Department of Defense or the U.S. Government.

**14. ABSTRACT**

There are longstanding interests in the analysis of explosive effects and applications in order to derive properties and predict an explosive's behavior. This work makes a contribution to the research field of metal acceleration by the means of detonations. The effects of both planar and convergent detonation fronts on metal acceleration are investigated with respect to the Gurney model. The derived characteristic velocity, the so-called Gurney constant, is material specific and characterizes the ability of metal acceleration for a certain explosive. The hydrocode program ANSYS AUTODYN is used to calculate and analyze the simulations of this work. The focus is set on cylinder expansion tests with respect to parametric variations. In addition, cylindrical coaxial charges are explored in order to compare the different methods of realizing a convergent detonation front. Experimental and simulated results are compared, discussed and evaluated.

**15. SUBJECT TERMS**

Gurney, cylinder expansion tests, convergent detonation front, AUTODYN, Andrews, coaxial charges

| **16. SECURITY CLASSIFICATION OF:** | | | **17. LIMITATION OF ABSTRACT** | **18. NUMBER OF PAGES** | **19a. NAME OF RESPONSIBLE PERSON** |
|---|---|---|---|---|---|
| **a. REPORT** | **b. ABSTRACT** | **c. THIS PAGE** | | | **19b. TELEPHONE NUMBER** *(include area code)* |
| Unclassified | Unclassified | Unclassified | UU | 103 | |

**Standard Form 298 (Rev. 8-98)**
**Prescribed by ANSI Std. Z39.18**

THIS PAGE INTENTIONALLY LEFT BLANK

**NAVAL POSTGRADUATE SCHOOL**
**Monterey, California 93943-5000**

Daniel T. Oliver
President

Leonard A. Ferrari
Executive Vice President and
Provost

The report entitled *"Investigation of the Effects of Convergent Detonation on Metal Acceleration and Gurney"* was submitted in partial fulfillment of the requirement for the degree of Master of Science from the Helmut-Schmid-Universität der Bundeswehr Hamburg.

**Further distribution of all or part of this report is authorized.**

**This report was prepared by:**

Wibke Ludwig
Visiting Researcher

**Reviewed by:**

Andres Larraza, Chairman
Physics Department

**Released by:**

Jeffrey D. Paduan
Vice President and
Dean of Research

THIS PAGE INTENTIONALLY LEFT BLANK

# ABSTRACT

There are longstanding interests in the analysis of explosive effects and applications in order to derive properties and predict an explosive's behavior. This work makes a contribution to the research field of metal acceleration by the means of detonations. The effects of both planar and convergent detonation fronts on metal acceleration are investigated with respect to the Gurney model. The derived characteristic velocity, the so-called Gurney constant, is material specific and characterizes the ability of metal acceleration for a certain explosive. The hydrocode program ANSYS AUTODYN is used to calculate and analyze the simulations of this work. The focus is set on cylinder expansion tests with respect to parametric variations. Crucial to this work is the implementation of an AUTODYN model suitable for the problem in question. In addition to cylinder expansion test simulations, cylindrical coaxial charges are explored in order to compare the different methods of realizing a convergent detonation front. With respect to this research, the experiment of Andrews et. al [1] has been set up in AUTODYN and has also been investigated through parametric modifications. The variation of sleeve thickness has been found to be substantial for the results. Experimental and simulated results are compared. Additionally, the effects of convergence on metal acceleration, respectively the Gurney constant, are discussed and evaluated for the Andrews experiment.

THIS PAGE INTENTIONALLY LEFT BLANK

# Table of Contents

# List of Figures

# List of Tables

# Erklärung

Hiermit versichere ich, Wibke Ludwig, dass ich diese Arbeit selbständig verfasst, keine anderen als die im Quellen- und Literaturverzeichnis genannten Quellen und Hilfsmittel, insbesondere keine dort nicht genannten Internetquellen benutzt, alle aus Quellen und Literatur wörtlich oder sinngemäß entnommenen Stellen als solche kenntlich gemacht habe und dass die auf einem elekronischen Speichermedium abgegebene Fassung der Arbeit der gedruckten entspricht.

Monterey, Kalifornien, den 13. Juni 2012

THIS PAGE INTENTIONALLY LEFT BLANK

# CHAPTER 1:
# Introduction

In this chapter, the research goal and the necessary background are explained in order to understand the work that is basis for this research. A short background is given to introduce the objectives and technical issues of this work.

## 1.1 Background

This research is based on the work of S. Andrews et al. [1] and partly on the work done by M. Sellam et al. [6]. Andrews examined the effect of detonation convergence on cylinder expansion and attempted to determine an effect on accelerating a disk. A copper cylinder, filled with PBXN-110, was set up. A hole was drilled in the cylinder and filled with PBXN-111. Therefore, the cylinder now was filled with two different detonating explosives. The sleeve explosive had a higher detonation velocity than the explosive in the core. Initiated by a Pentolite booster, the expansion of the cylinder was measured. Andrews tried to determine an effect on accelerating a steel disk at the end of the cylinder, but was unsuccessful due to the disk's fragmentation. In this experiment, a relatively thick sleeve of the fast detonating explosive was used to examine the effect of convergence. One result of his experiment is that the wall velocity of the cylinder, initiated by the ring charge of both explosives together, is almost as high as the wall velocity initiated just by a charge of PBXN-110. Sellam initiated overdriven detonation waves in nitromethane in order to measure velocities, pressure and brightness to compare these data to calculations. His research is important to the understanding of convergent detonation waves.

## 1.2 Technical Issues

Especially the work of Andrews motivates to alter his experiment and examine the effect of modified parameters. Among other things, the following points are of interest:

- Andrews used a relatively thick sleeve, which leads to a substantial mass regarding the cross section. Would one expect similar effects from thinner sleeves? The sleeve is the key factor in order to convert divergence into convergence, which makes it interesting to change the sleeve thickness in order to examine the effects.

- The convergent detonation front in Andrews' experiment was realized with a composite of two explosives with different detonation velocities. Is there another possibility of implementing a convergent front and what are the effects of it? In fact, there is the possibility of circumferential detonating points that create a convergent front in a charge of just one explosive.
- Concerning the acceleration of a steel disk, Andrews was not successful. The fragmentation made it impossible to examine any effects of coaxial charge on metal acceleration. As the experiment did not yield useful results in this area, simulations might be a way to overcome the problem of fragmentation and examine the effect of accelerating a metal disk and investigating the resulting energy.
- This work focuses on Gurney constants and the effect of convergence. Therefore, the overall effect of convergent detonation fronts on Gurney constants has to be examined. Another interesting topic is the energy partitioning: How is the energy distributed during detonation processes?

## 1.3 Research Goal and Objectives

Following the technical issues mentioned before, the goal of this work is to investigate the effect of convergence on metal acceleration and the Gurney constant. The question is whether there is a significant difference in results compared to divergent detonation waves and how that affects the Gurney constant. Therefore, objectives have been set in order to achieve this goal. These objectives have been investigated in this research.

- Examine and critique the Andrews experiment and validate computational techniques. Results of the experiment are compared to computational results and it is tried to overcome problems of the original experiment by simulations.
- Examine the effect of sleeve thickness. Andrews used a relatively thick sleeve and gathered valuable information about the effect on convergence by using a coaxial charge. Therefore, the effect of reducing sleeve thickness is investigated in this work.
- Examine the universality of the effect by using different explosives. Hence, the Andrews experiment was imitated with a charge of two other explosives. Furthermore, regarding the expansion test of the cylinder filled with only one explosive, three different explosives are examined.
- Examine the effect of all these parametric modifications on the Gurney constant.

## 1.4 Overview of Results

A short overview of the major results is presented in this section. Further information and results of every investigated configuration are documented in Chapter 5.

- The Gurney constant is a function of the ratio of the mass of the cylinder to the mass of the charge. There is a trend of decreasing Gurney constants as the mass ratio increases.
- Considering different sleeve thicknesses of coaxial charges and therefore different amounts of energy provided by the composite explosive, the Gurney constant is a function of this energy.
- There are at least two methods of implementing a convergent detonation front: An array of circumferential detonation points with an arbitrary sweep rate or arranging a coaxial charge of two explosives with different detonation velocities. The former does not appear to influence metal launching whereas the latter does.
- Regarding the circumferential detonation points, there is no major advantage of the convergent front regarding values of Gurney constants. This method of arranging a convergent front is found to be insufficient.
- The problem of investigating the effect of convergence on metal acceleration regarding a steel disk at the end of a cylinder could not be solved thoroughly due to the inevitable deformation of the disk. However, is was possible to clarify the difference between hydrocode simulations and theoretically derived equations regarding values of velocity. Theoretically derived equations such as Benham's equation do not regard the effects of deformation and leakage of the detonation products.
- The results of the experiment done by Andrews et al. [1] were validated.

THIS PAGE INTENTIONALLY LEFT BLANK

# CHAPTER 2:
# Technical Discussion

Detonation processes are based on the development of shock condition and rapid exothermic reactions that drive the shock through unreacted explosives. The effect of product gas formation associated with evolved thermal energy causes rapid gas expansion and exertion on adjacent bodies. As a result, the confinement expands outwards and other bodies in contact can be accelerated. In this chapter a short introduction into shock physics and detonation theory is given. A short review of the Gurney model and the cylinder expansion test is also presented in order to be able to follow the simulations. The essential problem of this work is the calculation of the Gurney constant that can be estimated in various ways. A method using the explosive's chemical structure is described in detail whereas other methods are just presented in their final outcome.

## 2.1 Shock Physics

The commonly used example to describe a shock wave in a material is the piston model. Suppose a cylinder that is open at one end and closed on the other end by a piston. The material in this cylinder is at rest. At a certain time, the piston begins to move and therefore drives the material to move at the same velocity. This process simulates the formation and transit of a shock wave through a material. The material in front of the shock wave is still at rest while the material behind the shock wave moves. To calculate a shock wave, five variables are required in their initial state in front of the shock (subscript 0) and their final state (subscript 1) just behind the shock front. The conservation laws for a single shock are:

$$\text{conservation of mass: } \frac{\rho_1}{\rho_0} = \frac{U-u_0}{U-u_1} = \frac{v_0}{v_1} \tag{2.1}$$

$$\text{conservation of momentum: } P_1 - P_0 = \rho_0(u_1-u_0)(U-u_0) \tag{2.2}$$

$$\text{conservation of energy: } e_1 - e_0 = \frac{P_1u_1 - P_0u_0}{\rho_0(U-u_0)} - \frac{1}{2}(u_1^2 - u_0^2) \tag{2.3}$$

where $\rho$ represents density, $U$ shock velocity, $u$ particle velocity, $P$ pressure and $e$ specific internal energy. Adding another equation, which is based on experimental results and expresses the relationship between shock and particle velocities, the Hugoniot equation can be acquired

by transforming the conservation laws into fixed coordinates, where the material in front of the shock is supposed to be at rest.

$$U = C_0 + su, \tag{2.4}$$

where $C_0$ is called the bulk sound speed and is a material constant just as $s$. This equation leads to a linear relation between the shock velocity $U$ and the particle velocity $u$ and applies to most explosives. Due to the number of variables, there are several planes in which these equations can be illustrated. The U-u plane, the P-v plane and the P-u plane were found to be the most useful planes. In most cases, the P-v plane is recommended for analyzing shock waves. The Hugoniot curve and the Rayleigh line in this plane are shown in Figure 2.1.

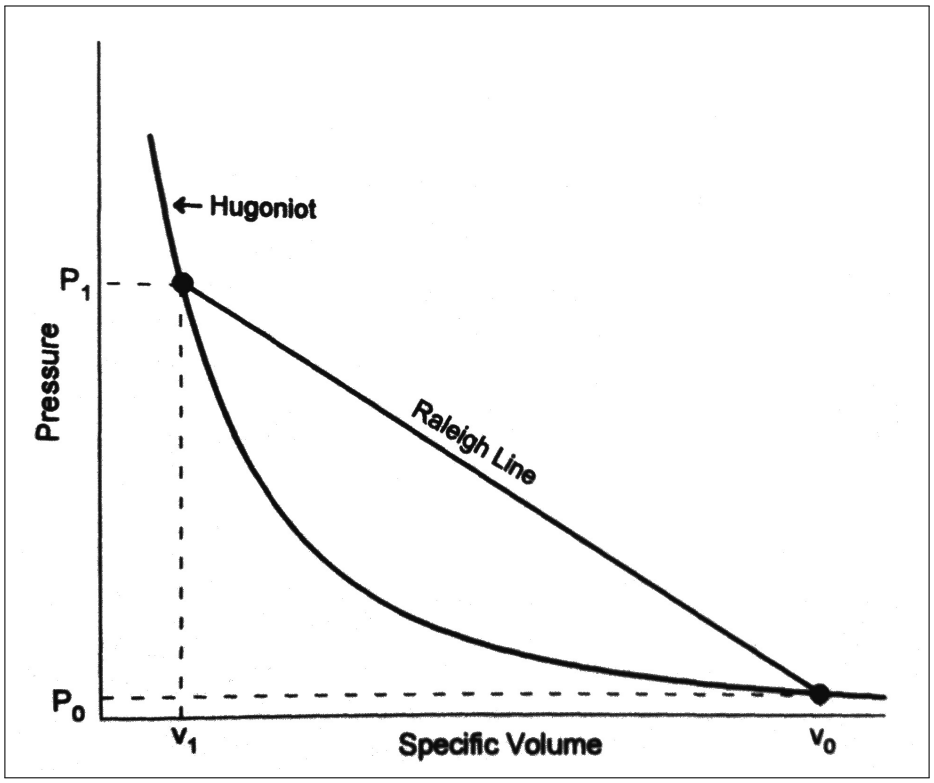


Figure 2.1: A typical Hugoniot curve with Rayleigh line in the P-v plane (from [2])

The Hugoniot curve represents every possible equilibrium state a material can exist. That does not imply a material moves along this line during a shock. The initial state of a shock is connected to the final state by the so called Rayleigh line. This line represents the jump condition a material goes through when it is shocked. The initial state of the material ($P_0$,$v_0$) and the state

after the shock ($P_1$,$v_1$) are highlighted in Figure 2.1. The equation of the Rayleigh line is

$$P_1 - P_0 = \frac{U^2}{v_0} - \frac{U^2}{v_0^2} v_1 \tag{2.5}$$

with the slope of $-\rho_0^2 U^2$. The equation of the Hugoniot line in this plane is

$$P = C_0^2 (v_0 - v) \left[ v_0 - s(v_0 - v) \right]^{-2}. \tag{2.6}$$

By knowing these equations, the P-v plane allows a number of calculations (from [2]):

- Calculation of the shock velocity if the initial and final P-v states are specified;
- Calculation of the final P-v state if the initial state and shock velocity are specified;
- Calculation of the final-state specific kinetic and internal energies if either the final P-v state or the shock velocity is specified;
- Calculation of the relief-wave energy changes.

## 2.2 Detonation Theory

A detonation wave traveling through an explosive can be handled as a shock wave implemented in inert material. This shock wave heats up and puts pressure onto the explosive which finally initiates the rapid chemical reaction. As a result of expanding detonation products, liberated energy keeps the detonation wave running while a rarefaction wave starts to move forward to the front. A full description of detonation waves includes closer consideration of many branches of science, e.g., thermodynamics, kinetics, shock physics. In order to get traceable mathematics, a simple model of ideal detonation has been developed independently from each other by Zeldovich, Von Neumann and Deering. As a consequence this model is called the ZND model or the "simple theory model". Basis of this theory are the following assumptions:

- The detonation wave is uniaxial, therefore infinite in one dimension and travels in normal direction in relation to its axis.
- The detonation front is discontinuous and is treated as the jump discontinuity of shock waves through inert material.
- The chemical reaction is completed instantaneously behind the detonation front. Product gases are in thermodynamic and chemical equilibrium.
- The length of the reaction zone is zero.

This model includes equilibrium of chemical reaction, detonation front and the rarefaction front. Therefore, both fronts move with the same velocity, the detonation velocity D. D and the pressure at the detonation front are independent of time and therefore do not change. Also the conservation laws mentioned in Section 2.1 apply to this model. The only difference concerns the conservation of energy. The thermal energy released during detonation adds to the specific internal energy change. Thus, a term of $+e_{detonation}$ is added to the energy equation for shocks in order to treat detonations. Regarding detonations, there are two materials to consider: the unreacted explosive as well as the detonation products. As a consequence, the P-v plane of a detonation contains two Hugoniot lines as shown in Figure 2.2. One for the equation of state (EOS) for the unreacted explosive and one Hugoniot for EOS of the reaction products. Beginning with the initial state (A), the state of the material jumps along the Rayleigh line to final state (C) as soon as the shock wave is formed.

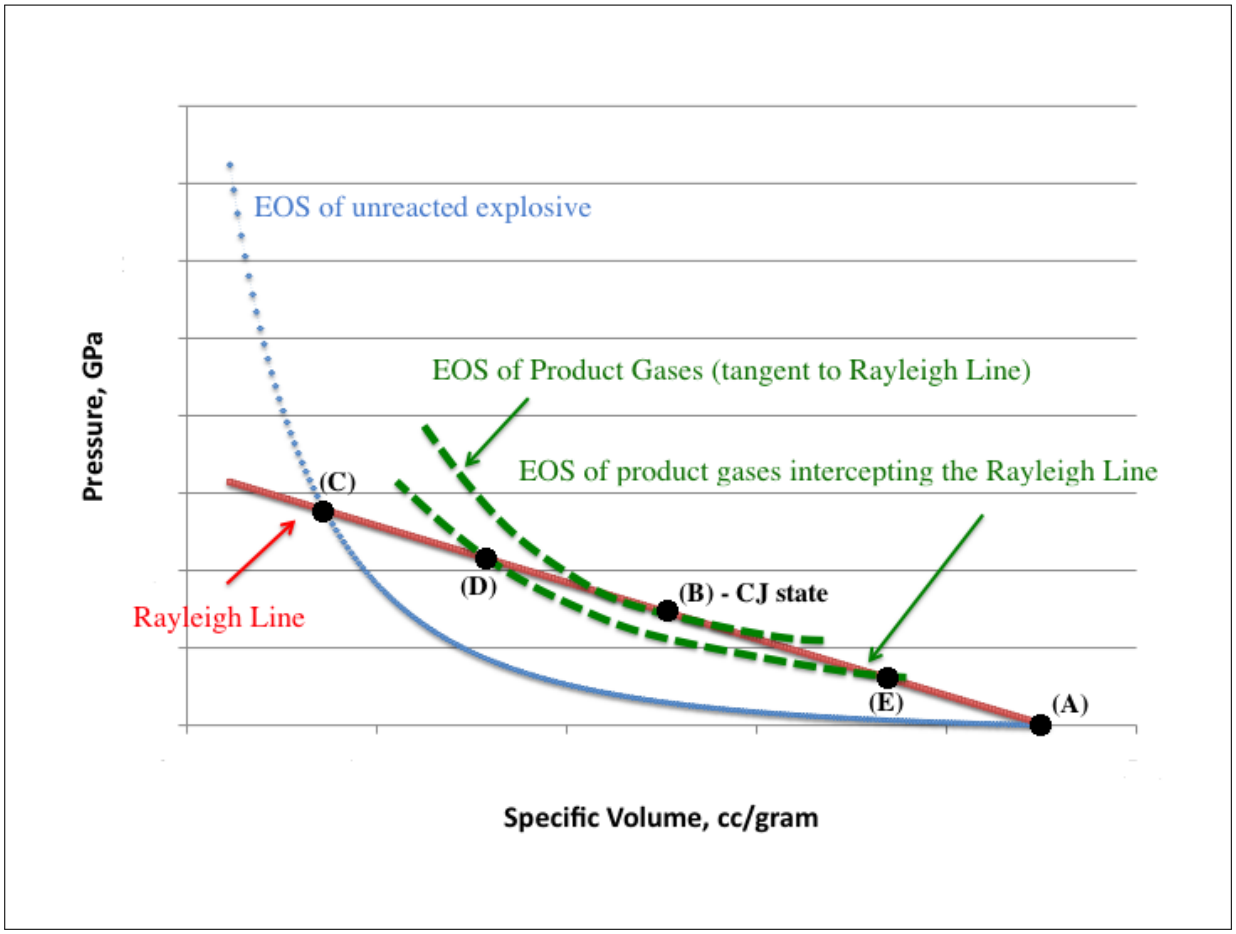


Figure 2.2: P-v plane showing Hugoniot and Rayleigh lines for a detonation

Due to the chemical reaction that is initiated with the detonation, detonation products are formed that have not the same Hugoniot as the unreacted explosive. State (B) correlates to a state of the detonation products on their Hugoniot. This state, which is called the Chapman-Jouget (CJ) state, is at a point where the Rayleigh line is tangent to that Hugoniot. Chapman and Jouget found this state to be the steady-state detonation condition. Although the length of the reaction zone is assumed to be zero, this is not true in reality. For most explosive the reaction zone has a thickness of $\tau < 1$ mm. In front of the reaction zone is the unreacted material, behind the zone are the detonation products and within the zone occurs the reaction. The CJ-state represents the rear of this reaction zone. If the Rayleigh line laid below products' Hugoniot, detonation products would not participate in the reaction and if it laid above, it would also not represent reality. Due to an inevitable formation of detonation products in reality the Rayleigh line must intersect with products' Hugoniot. If there were two intersections points, both states (D) and (E) would be possible. In point (D) the slope of the Hugoniot is greater than the slope of Rayleigh, which leads to a rarefaction wave faster than the shock front. The exact opposite would happen in point (E). A rarefaction wave slower than the shock front leads to the consequence of a reaction zone spreading steadily. Both, state (D) and (E) contradict the assumption of equal velocities. As a consequence the CJ-point represents the only possible state.

## 2.3 Overdriven Detonation

Overdriven detonations present a higher detonation velocity and a higher initial density than steady detonations. That leads to differences in the P-v plane, which are illustrated in Figure 2.3. This is a qualitative P-v plane for an overdriven detonation, containing the Hugoniot line for the unreacted explosive, the one for the detonation products and three different Rayleigh lines. The Rayleigh line for the unsupported steady-state detonation corresponds to the Rayleigh line of Figure 2.2. It is tangent to the product EOS. Due to the modified initial density and the higher detonation velocity of an overdriven detonation, the Rayleigh line shifts. A convergent front does not feature a consistent pressure profile along the front. This is the reason for the existence of more than one Rayleigh line. The qualitative minimum and maximum Rayleigh lines are displayed in Figure 2.3. As a consequence of the higher density, they start from a lower specific volume. Due to the higher detonation velocity and the higher initial density, the negative slope of the Rayleigh lines, $-\rho_0^2 D^2$, increases ($\rho_{0\_overdriven}^2 D_{overdriven}^2 > \rho_0^2 D^2$). These lines are also tangent to the product EOS, but at higher pressures.

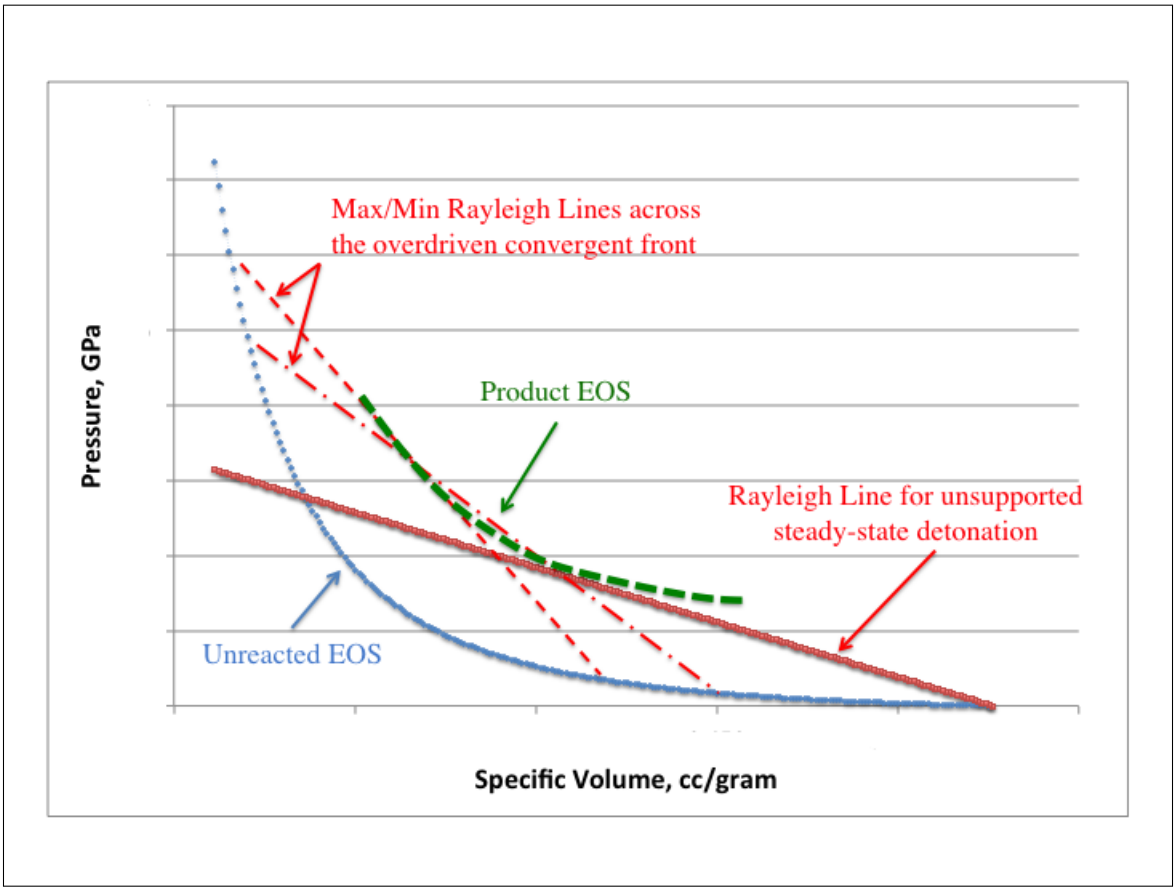


Figure 2.3: Rayleigh lines in a P-v plane for an overdriven detonation

## 2.4 The Gurney Model

The Gurney model was developed by R. W. Gurney, who was concerned with velocities of fragments from bombs, shells and grenades in order to compare efficiencies of fragmentation of different projectiles. He developed simple equations based on energy balance to estimate the final velocity of metal driven by detonation [7].

As engineers want to design projectiles or want to use detonations in general to accelerate metal, it is useful to provide particular impulses, acceleration or final velocity for the considered setup. These parameters highly depend on the geometry of the experiment, the materials that are used and their properties such as the initial density. The equations derived by Gurney base on some energy assumptions and lead to reasonable results. Concerning projectiles, the interesting velocity is the final velocity of the casing, regardless of the geometry. Gurney derived equations for simple projectile geometries, such as a cylinder or a sphere. However, these equations can

be expanded and therefore applied to more complicated geometries. The important variable of his equations is the energy E, which can be considered as a characteristic parameter for each material. The so-called Gurney constant ($\sqrt{2E}$) then has the dimension of a velocity and is therefore also called the characteristic Gurney velocity. Gurney's model bases on these assumptions:

- The kinetic energy is partitioned between the metal and the detonation product gases.
- The chemical reaction of the detonation proceeds instantaneously, i.e., there is an instantaneous energy release.
- Energy E is independent from the system's configuration and the size of the projectile.
- Under optimum conditions of detonation a certain fraction of the chemical energy of an explosion is converted into kinetic energy. The energy released by the chemical reaction is converted into kinetic energy of the metal fragments.
- The velocity of the metal is assumed to be constant throughout its thickness.
- Side or end losses of the different geometries are negligible.
- The gas velocity distribution is linear.

Beginning with the assumption of linear velocity distribution and regarding the energy and momentum balance, the following equations can be derived:

For a cylindrical casing filled with explosive:

$$\frac{V}{\sqrt{2E}} = \left(\frac{M}{C} + \frac{1}{2}\right)^{-1/2} \tag{2.7}$$

For a metal sphere filled with explosive:

$$\frac{V}{\sqrt{2E}} = \left(\frac{M}{C} + \frac{3}{5}\right)^{-1/2} \tag{2.8}$$

For a symmetric sandwich configuration, which refers to a plane explosive surrounded by two metal plates, where each metal plate has the mass M:

$$\frac{V}{\sqrt{2E}} = \left(\frac{2M}{C} + \frac{1}{3}\right)^{-1/2} \tag{2.9}$$

For an open face sandwich, which is equal to the symmetrical sandwich but with only one metal plate at one side:

$$\frac{V}{\sqrt{2E}} = \left( \frac{1+(1+2\frac{M}{C})^3}{6(1+\frac{M}{C})} + \frac{M}{C} \right)^{-1/2} \tag{2.10}$$

An important advantage compared to other methods of predicting velocities is the simplicity of the equations. Gurney managed to derive a simple coupling between the Gurney constant and the ratio of the mass of metal (M) over the mass of charge (C) an the nominal uncertainty of results is only 10% [8]. The Gurney model has been shown to compare very well with experimental data.

Despite the assumption of negligible side and end losses in theory, these effects cannot be neglected in real experiments. These losses may decrease the value of $\sqrt{2E}$ by up to 20% [9]. These 20% are a guide value for estimating the ideal value of $\sqrt{2E}$ from effective values measured in experiments with tremendous side losses. These losses may occur during early fragmentation of the metal. Early fragmentation is an issue of this work regarding the variation of the M/C ratio. It has to be stated, that this limitation (20 %) only refers to experiments with enormous side or end losses and does not refer to cylinder expansion tests in general.

Although the original Gurney equations are theoretically independent of size, which does not necessarily correspond to real experiments, Weinland[1] investigated the effect of scaling by analyzing the ratio of length over diameter (L/D) for open ended tubes. As a result, he stated that as long as L/D $\geq 6$, the values of $\sqrt{2E}$ are not effected by scaling. For ratios L/D $< 6$ the value of $\sqrt{2E}$ decreases and does not represent the theoretically possible Gurney energy any more.

There are further limitations of the applicability of the Gurney equations which have to be considered. Table 2.1 summarizes the most important limitations, which refer to this work. This table is compendious and refers to Table 1 in [8]. Expect for the first case, these limitations result from the assumption of instantaneous energy release.

The Gurney model applies to simple metal acceleration. In the following paragraph, the subject of effective charge is broached in order to introduce the purpose of a short simulation series that was done during this research. Concerning the open-face-sandwich configuration, tremendous side losses occur due to the lack of confinement around the charge.

[1] C. E. Weinland "A Scaling Law for Fragmenting Cylindrical Warheads", NWC TP 4735,China Lake, CA, April, 1969.

[2] I. G. Henry, "The Gurney Formula and Related Approximations for High-Explosive Deployment of Fragments", presented to the A.O.A., April, 1967.

Table 2.1: Limitations for the applicability of Gurney

| Restriction | Remarks and Recommendations |
|---|---|
| Range of M/C ratio | Henry[2]recommends restriction to the range of $0.2 < \text{M/C} < 10$ for velocity calculations. |
| Acceleration Phase | Gurney method is not capable of analyzing motion during acceleration. Acceleration is completed after detonation products have expanded to twice that original charge volume for incidence of detonation onto metal |
| Direction of Detonation Propagation | Detonation drives metal at a given velocity, within a few percent, for a given M/C regardless of the angle between the detonation front and the metal surface. |
| Gas velocity profile inaccuracy | Assumed linear velocity profile and constant density are gross oversimplifications. This assumptions ignores for example the effect of rarefaction waves. |
| Metal strength effects | No forces exerted by the metal to oppose deformation are considered, other than inertia. |
| Early case fracture | Leakage of product gases through fractures in the metal case can decrease the final metal velocity by no more than 10%. |

Taking a cylindrical charge with a metal plate at the end as an example for the open-face-sandwich configuration, it has been found that an effective length of charge exists. Only the effective part of the whole charge makes a major contribution to metal acceleration. This effective charge is a cone with 60° base angle and base diameter equal to charge diameter. In order to improve the setup and achieve higher velocities of the plate, metal side tamping can be provided. In order to treat this, Benham [10] extended the previous model of the 60° cone to

$$\Theta = 90 - \frac{30}{(2\Psi/C+1)^{0.5}} \tag{2.11}$$

where $\Theta$ is the base cone angle, which can be arbitrarily chosen depending on the examined problem, and $\Psi$ is the mass of the tamping cylinder. C in this equation refers to the full charge of explosive. The base cone angle is not set at a certain value but can be modified depending on the mass of the tamping cylinder.

### 2.4.1 Cylinder Expansion Test

All hydrocode simulations in this work are based on the cylinder expansion (cylex) test, hence it is advisable to provide a short description. In order to work with the equations of detonation theory, some of the required parameters, e.g., detonation velocity and CJ-pressure, have to be determined through experiments. Main purpose of the cylinder expansion test is to gather information about a certain explosive and therefore be able to predict explosive effects. The test is employed primarily for estimating the JWL (Jones-Wilkins-Lee) equation of state parameters but can also be useful for solving engineering problems. In addition, pressure and heat of detonation can be calculated by means of this test [3]. The experimental set-up is described by several authors [3, 11]. Basically, the experiment consists of a copper cylinder filled with a certain explosive.

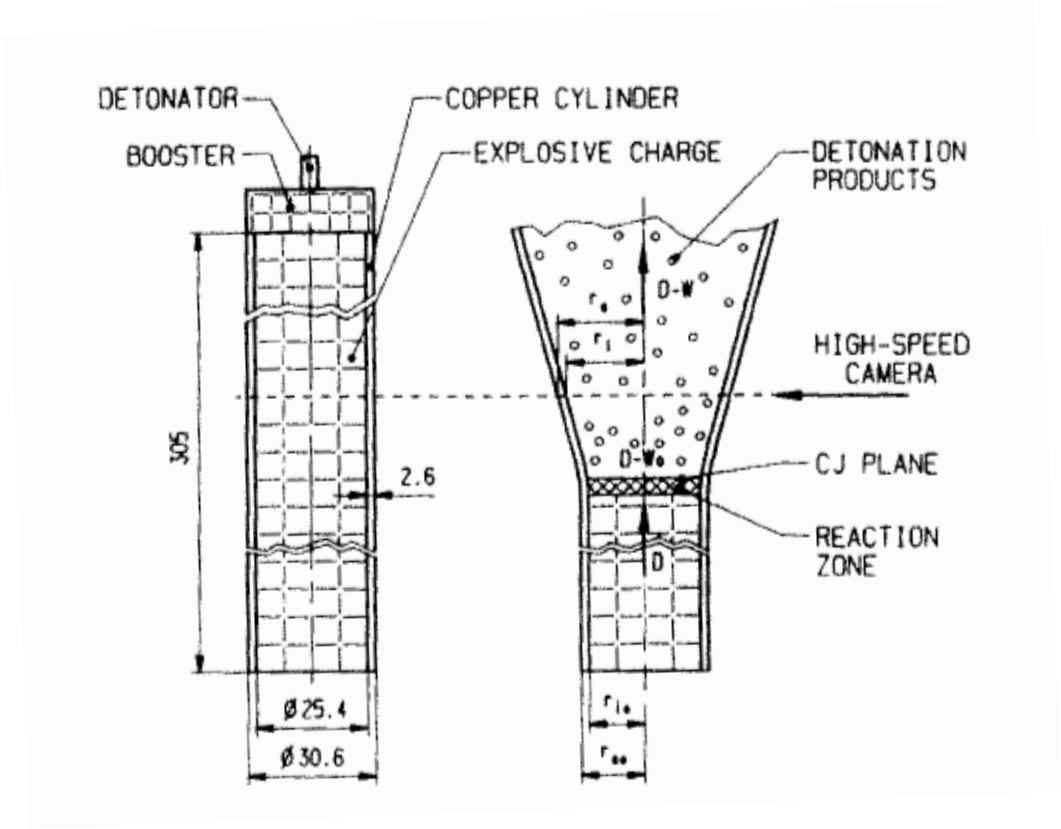


Figure 2.4: Cylinder expansion test setup (copied from [3])

Oxygen-Free High Conductivity (OFHC) copper is used because of its good dynamic ductility and resistance to tensile failure. Mostly optical measuring equipment is installed to gather the required information and results. In some cases there is a metal disk at the end of the cylinder

that is accelerated by the energy of the detonation. A cylinder design common for this particular kind of experiment has a length of 305 mm (12 in.), an inner diameter of 25.4 mm (1 in.) and a wall thickness of 2.6 mm (0.1022 in.). The general approach for conducting the cylinder expansion test is shown in Figure 2.4. Due to the lack of standardization, other geometries are available, most of them cylinders of larger dimensions. In this work a cylinder with the geometries of Andrews et al. [1] was used. This cylinder also is 305 mm long, but it is 50.8 mm in diameter and its thickness too was doubled to 5.2 mm.

In some cases there is an additional booster to initiate the charge. Once the charge is ignited and the detonation wave starts to travel through the cylinder, the expanding gaseous detonation products force a radial motion of the cylinder walls. This motion is measured mostly by optical measurements. Data gained from this test could be an expansion curve (cylinder radius vs. time curve). As mentioned before, the Gurney energy proved itself to be a property worth known for an explosive. Gurney provided an equation for a cylindrical setup (Equation 2.7), which makes it easy to calculate the Gurney energy with the cylinder expansion test. In this work the final cylinder wall velocity was measured by AUTODYN and used to calculate Gurney constants for different explosives.

## 2.5 Koch Treatment

There is a number of ways for empirically estimating the Gurney constant. In this section the way derived by Koch et al. [12] is described. Considering basic equations of thermodynamics and detonation theory, they deduced a link between the detonation velocity of an explosive and its Gurney energy: $\sqrt{2E} = D/3.08$. The method they used to derive this equation describes three configurations of the Gurney model. The symmetrical sandwich configuration, the cylindrical metal casing filled with an explosive and the sphere of inert material filled with a charge. To avoid long calculations the asymmetrical sandwich is excluded. Therefore, an explosive charge with the mass $C$ and an inert material, usually metal, with its mass $M$ are considered. A major simplification is taken by assuming the density and pressure of the detonation gases are homogeneous at all times. This does not represent reality but simplifies calculations and is consistent with a basic assumption of the Gurney model. At initiation time $t = 0$ all energy in the system is stored as internal energy $E_0$ of the gaseous products. As $t$ increases, the energy is distributed among three terms:

$$E(t) = E_{int}(t) + E_{kin}(t) + E_{case}(t) \tag{2.12}$$

$E_{int}(t)$ is the internal energy of the gas, $E_{kin}(t)$ the kinetic energy of the gas and $E_{case}(t)$ represents the kinetic energy of the metal case. Assuming an adiabatic relaxation, each of the above terms can be replaced.

$$E_{int}(t) = \frac{C}{\gamma - 1}\frac{P_0}{\rho_0}\left(\frac{R_0}{R(t)}\right)^{n(\gamma-1)} \tag{2.13}$$

$$E_{kin}(t) = \frac{nC}{n+2}v(t)^2 \tag{2.14}$$

$$E_{case}(t) = \frac{M}{2}v(t)^2 \tag{2.15}$$

$P_0$ and $\rho_0$ describe the initial pressure and density of the detonation gases. $R_0$ is the initial dimension of the inert case. That is either the initial radius of the explosive charge regarding both the cylindrical and spherical configuration or the explosive's thickness for the symmetric sandwich. Accordingly, $R(t)$ represents the expansion of the case at time $t$. $\gamma$ corresponds to the polytropic exponent and $v(t)$ to the velocity of the case relative to the initiation zone. The configurations are initiated at their center lines or their symmetrical planes, respectively. $n$ depends on geometry: symmetric sandwich: $n = 1$, cylindrical configuration: $n = 2$ or spherical: $n = 3$. By putting (2.13), (2.14) and (2.15) in (2.12) and assuming the internal energy of the gas at $t = 0$ as

$$E_0 = \frac{C}{\gamma - 1}\frac{P_0}{\rho_0} \tag{2.16}$$

the deduced equation can be transposed to receive $v(t)$ as a function of $R(t)$:

$$v(t) = \sqrt{\frac{\frac{2}{\gamma-1}\frac{P_0}{\rho_0}}{\left(\frac{n}{n+2}+\frac{M}{C}\right)}}\left[\left(1-\frac{R_0}{R(t)}\right)^{n(\gamma-1)}\right]^{1/2} \tag{2.17}$$

In order to derive a link between the detonation velocity of an explosive and its Gurney energy the next step is to consider the pressure. Using simple equations of detonation velocity and assuming an immediate and adiabatic relaxation of the detonation products directly behind the detonation front one can easily get a link between the homogeneous pressure $P_0$ and the Chapman-Jouget pressure $P_{CJ}$ of the detonation front:

$$P_0 = \left(\frac{\gamma}{\gamma-1}\right)^{\gamma} P_{CJ} = \frac{\rho_0}{\gamma+1}\left(\frac{\gamma}{\gamma+1}\right)^{\gamma} D^2 \tag{2.18}$$

$D$ is the detonation velocity of the explosive. In order to consider the final asymptotic velocity $v_\infty$ of the case, Equation 2.18 is introduced in 2.17 and the limit $t \to \infty$ is taken:

$$v_\infty = \sqrt{\frac{2E}{\left(\frac{n}{n+2} + \frac{M}{C}\right)}} \tag{2.19}$$

where $E$ is defined as

$$E = \frac{1}{\gamma^2 - 1}\left(\frac{\gamma}{\gamma+1}\right)^\gamma D^2 \tag{2.20}$$

This is the simple link between detonation velocity $D$ and Gurney Energy $E$. For most explosives the polytropic exponent can be presumed to be $\gamma = 3$:

$$E = \frac{27}{512}D^2 \approx \frac{D^2}{19} \tag{2.21}$$

Therefore the Gurney constant can be written as

$$\sqrt{2E} \approx \frac{D}{3.08} = 0.325D \tag{2.22}$$

Koch and co-workers compared their derived estimate of the Gurney constant to experimental values from literature. The largest derivation of the considered explosives are –9% for PETN and +5% for PBX9502. The average deviation is equal to 2%.

## 2.6 Further Empirical Estimates

Besides Koch, other investigators derived different approximations. Cooper [2] deduced a simple estimate just containing the detonation velocity D and a constant. As a consequence of the lack of any further explosive properties, this method applies to many explosives that are used in practice.

$$\sqrt{2E} = D/2.97 = 0.337D$$

The constant 2.97 was gained by calculating the mean value of $D\sqrt{2E}$ for a number of explosives [3]. A simple method which provides good estimates.

A further estimate of the Gurney constant was derived from gas dynamic analysis by Roth[4]. He proposed an approach based on the polytropic equation of state of the product gases. In addition

[3] see Table 27.1 in [2]

[4] Although this estimate was not published, the reference was found in [13].

to the detonation velocity, the polytropic equation of state exponent $\gamma$ has to be provided. For many explosives the assumption of $\gamma = 3$ leads to good results in the first place.

$$\sqrt{2E} = \frac{0.605}{\gamma - 1} D = 0.303D$$

### 2.6.1 Estimates of the Gurney Constant by Using Chemistry

Other methods for estimating Gurney constants for pure explosives and mixtures of explosives (exclusively additives) are based on Kamlet and Jacobs [14]. A number of investigators have used approaches based on their equations. Their goal was to be able to estimate detonation properties simple and quick without using computational resources. They deduced some semi empirical equations for C-H-N-O explosive that allow further estimates of detonation properties:

$$P = K\rho_0^2\Phi \qquad K = 15.58 \qquad \Phi = NM^{1/2}Q^{1/2} \tag{2.23}$$

and

$$D = A\Phi^{1/2}(1 + B\rho_0) \qquad A = 1.01 \qquad B = 1.30 \tag{2.24}$$

where $P$ is in kilobars, $D$ in millimeters per microsecond, $N$ in moles of gas per gram of explosive, $M$ in grams of gas per mole of gas, $Q$ in calories per gram and $\rho_0$ in grams per cubic centimeter. $D$ depicts the detonation velocity and $\rho_0$ represents the initial density of the explosive. Therefore, the only input to calculate detonation properties are the initial density and the parameters $Q$, $M$ and $N$, which are based on apparent (or assumed) detonation reaction, where $CO_2$ is the preferred oxidative product from the reaction between carbon and oxygen. To estimate the heat of detonation ($Q = -\Delta H_0$) correctly for this method, one has to consider the explosive's decomposition during detonation. Kamlet and Jacobs assume for a $C_aH_bN_cO_d$ explosive the predominant formation of carbon dioxide rather than carbon monoxide:

$$C_aH_bN_cO_d \rightarrow {}^1\!/_2 bH_2O + {}^1\!/_2 cN_2 + \begin{cases} ({}^1\!/_2 d - {}^1\!/_4 b)CO_2 + (a - {}^1\!/_2 d + {}^1\!/_4 b)C & \text{if underoxidized,} \\ aCO_2 + ({}^1\!/_2 d - {}^1\!/_4 b - a)O_2 & \text{if overoxidized.} \end{cases}$$

Calculated values by Kamlet and Jacobs matched predicted values of detonation properties by computer code RUBY. As already mentioned, these equations can be used to estimate Gurney velocities.

Hardesty and Kennedy [15] extended the use of the parameter $\Phi$. Chapman-Jouget pressure $P_{CJ}$, detonation velocity $D$ and detonation energy $Q$ are not the only important factors for predicting detonation performance. Based on the work of Kamlet et al., Hardesty and Kennedy emphasize the importance of an energy by that imparted velocities and impulses to metal can be calculated. They used the TIGER computer code and the JCZ3 (Jacobs-Cowperthwaite-Zwisler) equation of state. Following Kamlet's idea of linking properties to fundamental chemical structures, Hardesty and Kennedy observed that the ratio of detonation pressure $p$ and loading density $\rho_0$ may be treated as a specific kinetic energy because of the dimensions.

$$c^* = \sqrt{P_{CJ}/\rho_0} = \sqrt{1.44\Phi\rho_0} \tag{2.25}$$

Plotting the Gurney energy against this specific kinetic energy for a number of explosives they managed to derive from a single linear least squares correlation the link between Gurney and Kamlet $\Phi$.

$$\sqrt{2E} = 0.6 + 0.54\sqrt{1.44\Phi\rho_0} \tag{2.26}$$

Kamlet and Finger [16] presented an alternative method for calculating Gurney velocities. They fitted computer code and cylinder test results done by the Lawrence Livermore Laboratory.

Even so the approximation of Hardesty and Kennedy produced good results compared to computer code TIGER, they derived another equation:

$$\sqrt{2E} = 0.887\Phi^{0.5}\rho_0^{0.4} \tag{2.27}$$

They compared their predicted values to results calculated by the Hardesty-Kennedy method and the TIGER code. It is shown that their simpler equation gives a more closer approximation to measured results.

What this all amounts to is that Gurney constants can be estimated for a number of explosives by just considering chemical structure. Even if these methods seem to provide good results compared to computational calculations and experiments, a problem may be detonation heat values. They depend on the equilibrium of chemical reactions which cannot be predicted exactly. Therefore the heat of detonation can differ by more than 100%, dependent on the initial density and the confinement of the vessel in which the explosive is detonated [17].

### 2.6.2 Overview of Estimates and Reference Data

There are several ways to estimate the Gurney constant of an explosive. Two ways have been presented in this section in detail. An overview of current estimates for the Gurney constant is listed with their references in Table 2.2.

Table 2.2: Overview of current estimates for the Gurney constant

| Reference | Calculation |
|---|---|
| Koch et. al [12] | $\sqrt{2E} = \frac{D}{3.08} = 0.325D$ |
| Hardesty and Kennedy [15] | $\sqrt{2E} = 0.6 + 0.54(1.44\Phi\rho_0)^{0.5}$ |
| Kamlet and Finger [16] | $\sqrt{2E} = 0.887\Phi^{0.5} + \rho_0^{0.4}$ |
| Roth [13] | $\sqrt{2E} = \frac{0.605}{\gamma - 1}D = 0.303D$ |
| Cooper [2] | $\sqrt{2E} = \frac{D}{2.97} = 0.337D$ |

Gurney energies for each explosive used in this work, employing all aforementioned approximations are presented in Table 2.3 and Table 2.4. The reference densities and detonation velocities in Table 2.4 were taken from the AUTODYN library. Using the example of HMX, the calculation of $\Phi$ is listed in the Appendix. The result of every simulation in this work will be compared to the values listed in these tables. Table 2.5 contains a number of Gurney constants that were found in textbooks and articles. Some values were obtained experimentally and others were calculated by different hydrocodes.

Table 2.3: Gurney constants calculated by various techniques based on $\Phi$

| | Parameters for $\Phi$ | | | | Gurney constant using | |
|---|---|---|---|---|---|---|
| Explosive | M | N | Q | $\Phi$ | Hardesty | Kamlet |
| | [g/mole] | $\left[\frac{\text{moles gas}}{\text{gram explosive}}\right]$ | [cal/g] | | & Kennedy | & Finger |
| TNT | 28.54 | 0.02532 | -1088.7 | 4.46 | 2.35 km/s | 3.09 km/s |
| HMX | 27.2148 | 0.03376 | -1618.17 | 7.08 | 2.97 km/s | 3.65 km/s |

Table 2.4: Gurney constants calculated by various techniques based on the detonation velocity

| | Explosive | | | | | Unit |
|---|---|---|---|---|---|---|
| | Lx-14 | TNT | HMX | PBXN-110 | PBXN-111 | |
| reference density $\rho_0$ | 1.835 | 1.63 | 1.891 | 1.672 | 1.780 | [g/cm$^3$] |
| detonation velocity D | 8.8 | 6.93 | 9.11 | 8.311 | 5.775 | [km/s] |
| equation of | Gurney constant | | | | | |
| Cooper | 2.96 | 2.33 | 3.07 | 2.80 | 1.94 | [km/s] |
| Koch | 2.86 | 2.25 | 2.96 | 2.70 | 1.875 | [km/s] |
| Roth | 2.66 | 2.10 | 2.76 | 2.51 | 1.75 | [km/s] |

Table 2.5: Gurney constants gathered from literature

| Explosive | Density $[g/cm^3]$ | Gurney [km/s] | $\Phi$ | Reference | Remarks |
|---|---|---|---|---|---|
| TNT | 1.63 | 2.37 | | [2] | origin of difference of these three values not specified |
| | 1.63 | 2.44 | | [2] | |
| | 1.63 | 2.46 | | [2] | |
| | – | 2.33 | | [18] | |
| | 1.63 | 2.37 | | [12] | |
| | 1.63 | 2.37 | 4.868 | [15] | |
| | 1.625 | – | 4.838 | [17] | $\rightarrow$ Hardesty/Kennedy: 2.42, Kamlet/Finger: 3.17 |
| HMX | – | 3.17 | | [18] | |
| | 1.89 | 2.97 | | [12] | |
| | 1.903 | – | 6.776 | [17] | $\rightarrow$ Hardesty/Kennedy: 2.93, Kamlet/Finger: 3.60 |
| | 1.89 | 2.97 | 6.768 | [15] | |
| | 1.835 | 2.80 | | [2] | |
| LX-14 | – | 2.80 | | [19] | |
| | 1.83 | 2.35 | | [20] | Gurney constant calculated from given radius-time history |
| | 1.835 | 2.80 | | [12] | |

## 2.7 Hydrocode Simulations

Hydrocodes are a powerful tool to numerically simulate high stress and high strain events, such as shocks or detonations. These computer codes are able to model the behavior of continuous fluid flows with respect to the principles of conservation of mass, momentum and energy. Due to the fact that rigid materials behave as fluids under high stress events, these programs are suitable for detonation problems. The solutions to these kind of complex problems cannot be obtained analytically due to the large amount of equations, which have to be solved simultaneously. Therefore, numerically obtained solutions are the only possibility. Based on the limited memory of a computer, which can only represent continuous problems by cutting it into pieces, a discretization technique is required [21]. Discretization is realised through a mesh, which divides the model of the simulation into pieces. These pieces are the cells. During each cycle of calculation, each cell is calculated with all necessary variables. In addition, boundaries are required in order to control the calculation.

Mesh generation algorithms depend on the solver and additional inputs from the user. The two most applied solvers are the Lagrangian and the Eulerian solvers. Lagrangian represents a material description and Eulerian corresponds to a spatial description [22]. The main difference is the generation of the mesh. When using the Lagrange solver, the mesh is connected to the parts of the model. Therefore, the mass within a cell is constant at all times. As a consequence, the mesh deforms with the material, which can lead to highly distorted cells. The timestep of the calculation, respectively the total computing time, depends on the smallest cell of the model. Hence, severe cell deformation can cause small timesteps and even an early termination of the calculation. There is the option of rezoning a mesh in order to avoid the timestep from decreasing, but the rezoning has to be done carefully so areas where a rezoning would be of significant influence have to be determined. However, the Lagrangian solver offers remarkable advantages. For example, a grid that is only generated where materials are in the model or the ability to follow a material's history.

An Eulerian solver uses a mesh that is at all times fixed in space. The cells are not connected to certain areas of the parts rather than to fixed coordinates in space. As a consequence, the cells always have a constant volume. Therefore, this solver calculates the flow of material through the mesh. The ensuing disadvantage of this solver is the indispensable generation of the grid, which has to be large enough to cover the whole area in which material flow may arise. The distinction between the two mathematical methods of the solvers are exemplified in [22] by

comparing the way of calculating the density of a cell. Due to the constant volume of each cell in the Euler solver, the mass would have to change in order to increase or decrease the density. The Lagrangian solver generates cells with a constant mass, therefore, the volume of the cell changes. The choice of the correct solver for a certain problem is crucial in order to gather accurate and reliable results.

### 2.7.1 AUTODYN Hydrocode

ANSYS AUTODYN is a multi-solver that has been shown to accurately predict the effects of blasts, hypervelocity impact, explosive detonation and explosively induced metal launching [23]. All simulations of this work were calculated with AUTODYN. Due to the approached detonation problems of this work, the Euler solver had been chosen. The differences between the most important solvers, Lagrange and Euler, has already been discussed in the above section. In addition, the advantages and disadvantages of AUTODYN's Euler solver are summarized in Table 2.6. Besides Lagrange and two Euler solvers, AUTODYN offers an ALE (Arbitrary Lagrange Euler) solver and a Mesh Free Solver, which uses a Smooth Particle Hydrodynamics Method. These solvers are not discussed further in this work.

The advantages and disadvantages of AUTODYN's Euler solver are summarized in Table 2.6.

Table 2.6: Advantages and disadvantages of the Euler solver (from [5])

| Advantages | Disadvantages |
|---|---|
| • No grid distortions<br>• Large deformation<br>• Mixing of initially separate materials<br>• Rezoning not required<br>• Erosion not required<br>• Larger time step in general | • More computations per cycle<br>• Need finer zoning for similar accuracy and extra cells for potential flow regions<br>• Shocks diffused more than Lagrange<br>• Less flexible for strength modelling<br>• Thin sections need small time steps |

THIS PAGE INTENTIONALLY LEFT BLANK

# CHAPTER 3:
# Nature of the Problem

In order to gather useful and comparable results, some challenges regarding the implementation of problems had to be overcome. An overview of examined configurations in AUTODYN is presented in this chapter with the corresponding problems and challenges.

The first step of this work was to implement a 5 cm charge cylinder expansion test. The exact model setup is described in Section 4.4. Using this setup, a parameter study was performed to detect effects on the Gurney energy. The ratio of the mass of the cylinder over the mass of the charge was varied over a number of values, as well as the quantity of single detonation points regarding the horizontal array of circumferential detonation points. In addition, three different explosives were investigated. Besides, details of the model itself and characteristics of AUTODYN, such as the difference between a direct and indirect detonation path, were regarded. As the cylex test was chief subject of this work, certain simulations were rerun with a larger cylinder (15 cm charge). Resolution and size are always issues of numerical problems, so the effect of scaling the cylinder as well as refining the numerical mesh had to be examined. The problem of size and resolution and the consequential results are depicted in Section 4.2. A number of problems occurred in this simulation series, which had to be overcome in order to gather reliable results from these simulations. The first and possibly most important problem is to a achieve a model in AUTODYN that runs without any error and represents the real experiment. At first, simulations were done with a resolution of one cell per millimeter in order to test the computational time. Due to the relatively short computational time of less than an hour, the resolution was increased to two cells per millimeter. Suddenly, the computations presented a very small timestep and ran for many hours. Problem of this configuration was the way of setting up the model in AUTODYN. For example, there are different ways in AUTODYN to fill an implemented part with material. It turned out that changing the method of filling the part, which is just another algorithm provided by AUTODYN and does not make any obvious difference to the user, saved computational time. The exact description of the model set up including the methods of filling a part are described in Section 4.4. Another challenge regarding the first calculations was to measure velocities accurately. The interesting outcome of each simulation is at least the velocity of the cylinder wall in order to calculate the Gurney constant. In the course of this research several methods of measuring velocities were tested and compared.

The detailed description of these methods is listed in Section 4.1. Anticipating the result, fixed gauges compared to moving gauges seem to be more accurate in order to measure velocities.

Result of these cylex simulations are the change of Gurney constants, respectively final wall velocities, concerning convergent detonation fronts compared to planar fronts caused by point initiation. Each simulation was performed with both shapes of detonation fronts. The convergent front evolves from an array of circumferential detonation points. Putting only one detonation point at the beginning of the cylinder leads to a spherical detonations front that later transforms into a planar front depending on the diameter and length of charge. Besides the correct size of the model parts and the resolution of the mesh, especially the peculiarities of AUTODYN, such as the different options of filling a part or implementing detonation paths had to be considered thoughtfully. During this simulation series, the importance of a model setup that corresponds accurately to the real experiment became evident. In fact, the whole cylex test series had to be iterated a number of times due to constant improvements to the model such as the different methods of filling the part or the use of gauges, as explained in the paragraph before.

Besides the cylex test, the main focus of this work refers to the experiment of Andrews. In order to analyze the effect of convergence it is worthwhile to consider numerical simulations of this experiment in order to validate results. A more detailed description of the experiment should be given here. A copper cylinder with an inner diameter of 50.8 mm is filled with two coaxial arranged explosives. PBXN-111 with a detonation velocity of 5.77 km/s was taken as the core, surrounded by a sleeve of PBXN-110 with a detonation velocity of 8.311 km/s. Due to the higher detonation velocity of the sleeve, this configuration always enforces a convergent detonation front. According to the original setup the sleeve is 12.9 mm thick. A booster charge of Pentolite is arranged at one end of the cylinder and a steel disk was put at the other end of the cylinder, in order to gather information about the effect of this configuration on metal acceleration. The final setup arranged in AUTODYN is shown in Figure 3.1 and the original setup is shown in Figure 3.2.

The material locations are illustrated in different colors and the detonation point in the booster is displayed. Although a more accurate description of the use of gauges is provided in Section 4.1, the arranged gauges in this configuration should be presented. There are moving gauges both in the cylinder wall (gauge 1–11) and in the steel disk (gauge 12–22). Two parallel arrays of fixed gauges are arranged in each explosive in order to measure the detonation velocity (gauge 106–110 in the core and gauge 111–115 in the sleeve).

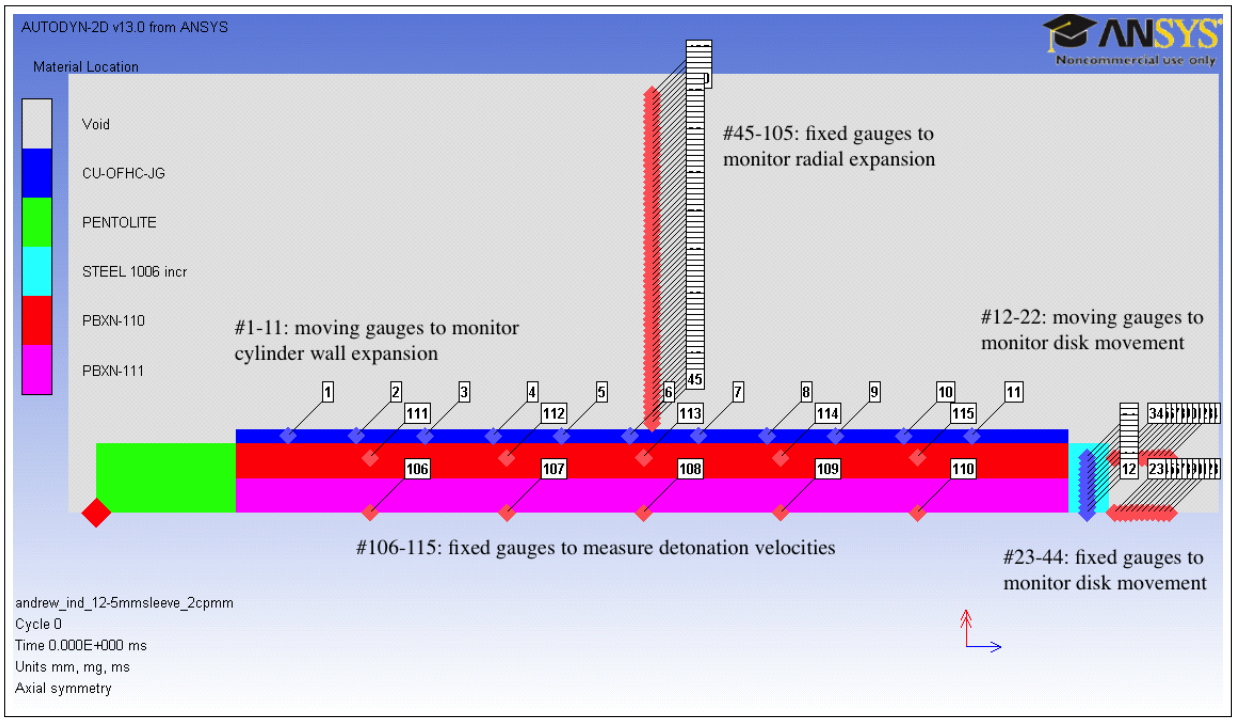


Figure 3.1: Setup of the Andrews experiment in AUTODYN

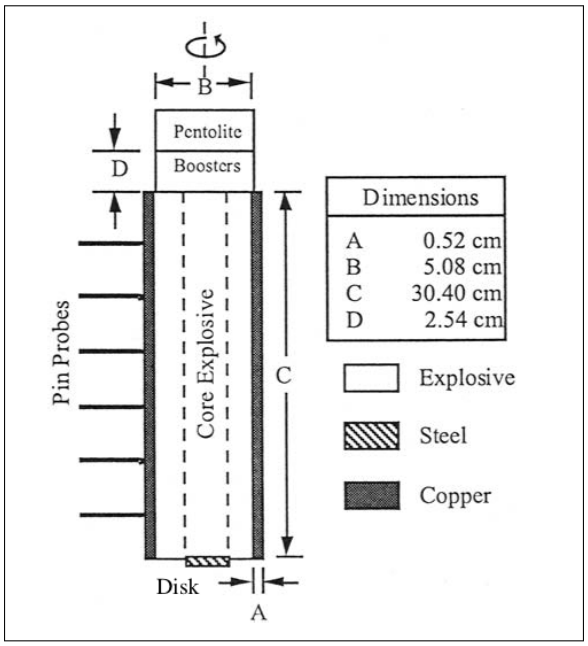


Figure 3.2: Setup of the experiment with the steel disk conducted by Andrews [1]

Additionally, two parallel arrays of fixed gauges are arranged behind the steel disk for the purpose of measuring its velocity (gauge 23–33 along the center line of the cylinder and gauge 34–44 at the upper edge of the disk). The velocity of the cylinder wall is measured by an array of fixed gauges that is arranged at the middle of the cylinder (gauge 45–105). In preliminary simulations three columns of arrays were arranged at regular intervals. The measured final velocities did not vary widely, so it was decided to just use one column in the middle of the cylinder. This column is always implemented in the same position, so results are comparable.

Andrews used a relatively thick sleeve with a substantial mass. The effect of sleeve thickness on the final velocity of the cylinder wall, respectively the Gurney constant was examined with consideration of the energy provided by the composite explosive. Beginning from the original thickness of 12.9 mm, the sleeve was stepwise reduced to 10 mm, 5 mm and 2 mm. Finally cylinders just filled with PBXN-111 or PBXN-110 were arranged to compare this data to data gained from setups with a sleeve. Hereby, the effect of energy is of special interest. Different contributions of the explosive to mass and volume result in different total energy provided by the composite. Therefore, an investigation of the coupling between total energy and Gurney had to be done. Due to the already existing data for this experiment, there is the possibility of comparing experimental data with the results of the simulations. Besides PBXN-111 and PBXN-110, a simulation series with a TNT core surrounded by a sleeve of LX-14 was analyzed in the same matter. Changing the explosives provides information about the universality of results. Besides, these results can be compared to the results of the TNT cylex tests with a convergent front implemented by circumferential detonation points.

In order to investigate the effect of convergence on metal acceleration, a steel disk was put at the end of the cylinder. Andrews was unsuccessful concerning this problem due to the fragmentation of his 9.53 mm disk during the experiment. A way to prevent the steel from fracture is to increase its yield stress. In addition, deformation of the disk is avoided as effectively as possible. Modeling the disk as a rigid body without deformation could not be achieved. As opposed to Andrews, the steel disk was enlarged up to the inner diameter of the cylinder and thickened up to 15 mm. The disk used by Andrews did not cover the whole charge. Due to the variation of sleeve thickness in this work, it was decided to enlarge the disk. The velocity of the disk was measured at two positions: at the center line of the cylinder and at the upper edge of the disk. Due to inevitable deformation, the velocities always differ from each other, which makes it difficult to determine a final velocity that applies to the whole disk.

Additionally, a number of simulations were computed with an unmodified steel disk to observe the deformation. The convergent front impinges upon the steel disk at its upper and lower edge at first, due to the front's geometry, whereas a planar detonation front collides with the disk at its whole surface. The highest pressure of the convergent front and therefore the highest obtainable force to drive the disk is found at the center line of the cylinder. That leads to significant deformations of the disk's center as time proceeds. Depending on charge diameter and disk thickness, it is possible to shatter the disk in the middle. In contrast, the pressure throughout the planar detonation front is constant. Hence, the plate is accelerated at its whole surface rather than locally at the center, which influences the total displacement of the disk. In addition, planar detonation fronts cause less deformation.

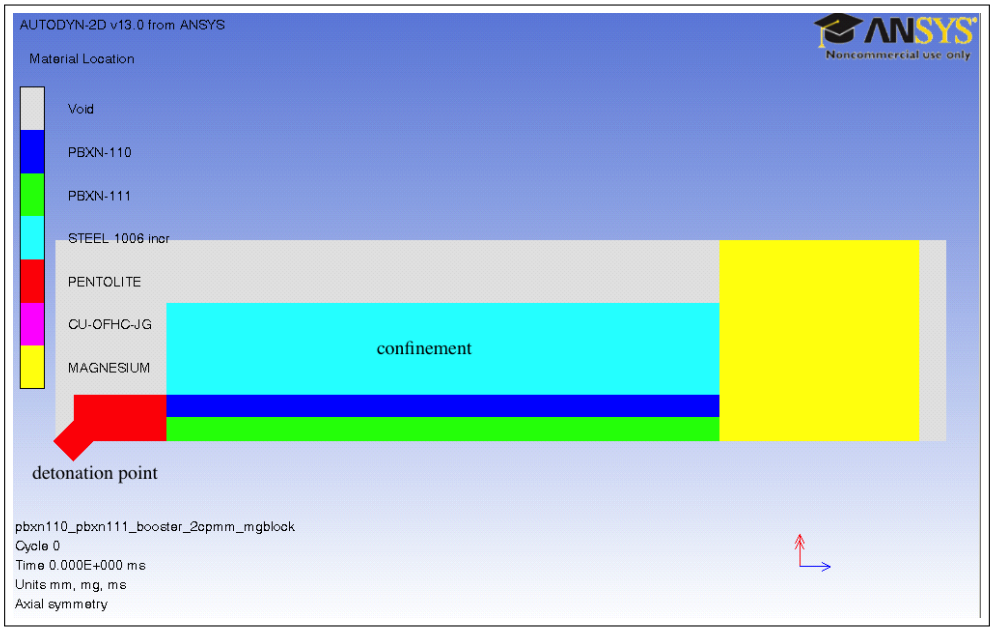


Figure 3.3: Modification of the Andrews experiment with a magnesium block

In order to get an idea of the outcome of such a detonation, the Andrews configuration was modified. A block of magnesium instead of a steel disk was put at the end of the cylinder, see Figure 3.3. As soon as the detonation front reaches the block, it burns a cavity in the magnesium. The cavity's depth as well as the changes of the magnesium's internal energy while the detonation front moves forward are of peculiar interest. Steel with an increased yield stress was used for the cylinder instead of OFHC copper in order to focus the energy in on the outcome of the cylinder[5].

[5]Results from this set of computations were compromised by not having a sufficient space between the target and the boundaries of the model for expansion

As a matter of fact, it exists an effective charge length, which is a fraction of the whole cylindrical charge, which has already been mentioned in Section 2.4. Therefore, only a certain part of the charge has an effect on a plate at the end of the charge. This theory corresponds to a cylindrical charge with a metal plate at the end and no casing, which is consistent with the open-face-sandwich configuration, mentioned in Section 2.4. Derived from experimental results, the effective length of a cylindrical charge has been found to be a cone with 60° base angle and base diameter equal to the charge diameter. To check this fact, a 305 mm cylinder was implemented in AUTODYN and steadily truncated. For a 5 cm charge the effective charge cone has to be 43.3 mm high based on Benham's model. In a short series of roughly implemented simulations, this effect was tested. This work contains exclusively cylindrical charges with casings. Hence, the extended equation of Benham (Equation 2.11) was worthwhile to implement in AUTODYN. In order to avoid an effect of size, a 16 cm charge was set up. The base angle of the cone was set to be nearly 90° in order to detect the limit of that model. Regarding the length of arbitrarily chosen 300 mm and a base angle of nearly 90°, the steel walls of the cylinder had to be 50 cm thick. Such a large model needs a lot of computing time even with a one cell per millimeter resolution. For that reason it was decided to not examine the Benham equation further in this work, although this theory is worth to verify in AUTODYN with a suitable model.

In summary, it can be stated that the crux of getting reasonable results is an accurate and suitable implementation of the problem in AUTODYN. Therefore, an exact description of one model of the cylex test series is given at the end of the next chapter.

# CHAPTER 4:
# Technical Approaches

To achieve the goals and objectives of this work, basic approaches were implemented in practice by use of the hydrocode AUTODYN. This chapter contains essentials of hydrocode simulations in general and specifics of ANSYS AUTODYN. Beforehand, details of how AUTODYN was used in this work are given, e.g., the special use of gauges and the implementation of convergence. The problems of size and resolution, which always are an issue of numerical calculations, are also covered.

## 4.1 Moving vs. Fixed Gauges

The goal of every simulation of this work is to measure velocities. These velocities can be obtained by either fixed or moving gauges arranged in the AUTODYN model. In the end, fixed gauges were found to be more useful for the different simulation configurations. The derivation of this result is presented in this section.

In order to analyze all simulations correctly and to be able to compare the results the meaningful use of gauges is important. The goal is to measure velocities, first of all the final velocity of the cylinder wall. Gauges can either be fixed or moving. They can be arranged in a vertical or horizontal array or set as single points. An obvious solution to the problem is an X-array of moving gauges in the middle of the cylinder wall. Theses gauges are not fixed in space so they can move with the material as it is expanded by the detonation wave. The final asymptotic velocity can then be read off the simulation's history. An option exists to show Y-velocity over time for certain gauges. Results are shown in Figure 4.1. The whole graph is displayed as well as an enlargement of the asymptotic graph of velocity. Figure 4.1 refers to a standard cylinder expansion test of a OFHC copper cylinder filled with LX-14 (5 cm charge in diameter). The M/C ratio is 2.2 and the cylinder is initiated by an array of circumferential detonation points. The whole setup is discussed in Section 4.4 and shown in Figure 4.9. It was calculated with a two cell per millimeter resolution. The numbering of the gauges corresponds to the numbering of Figure 4.9. The XY coordinates of gauge one are (20,28) and the other gauges follow in an interval of 25 mm in X direction. The cylinder is arranged at the origin of the coordinate system, so the first gauge is set in a distance of 20 mm from the beginning of the cylinder.

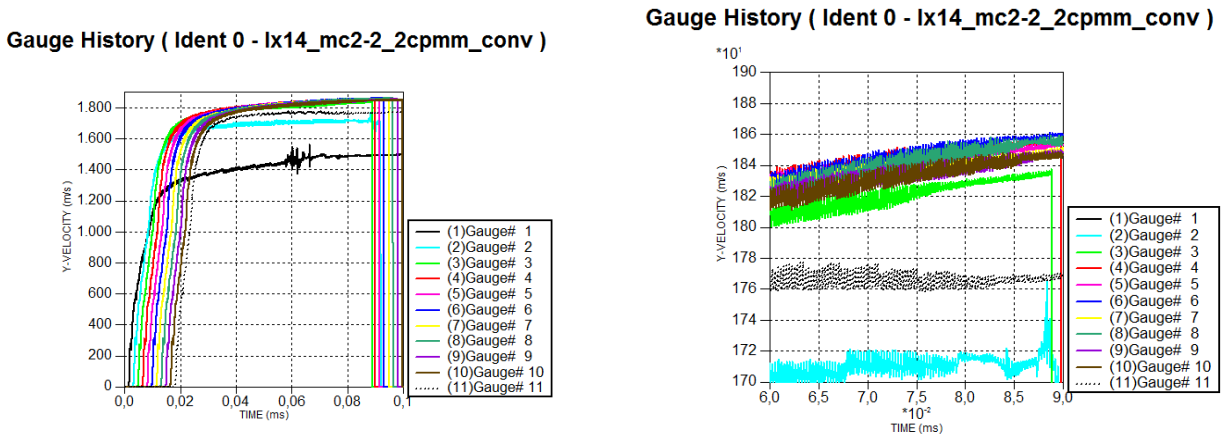


Figure 4.1: Y-velocity of the moving gauges in the cylinder wall surrounding a 5 cm charge of LX-14, M/C = 2.2, circumferential initiation points

In order to analyze Figure 4.1 and compare it to following figures, it is important to reflect that the M/C ratio is 2.2., i.e., the mass of the cylinder is 2.2 times the mass of the charge. It is not problematic to read the final asymptotic velocity off Figure 4.1. Gauge one and two, however, show a conspicuous course. Their final velocity is far below the other gauges' velocity. This is caused by the position of these gauges. Number one and two are positioned on the first 50 mm of the cylinder. Regarding the way of initiation, a convergent front is not stabilized at once. It takes a few initiation points and at least 50 mm to develop a stable convergent detonation front. Therefore, the cylinder wall is not accelerated equally. As soon as the gauges move out of the created model, there is a sudden decrease of velocities because no more parameters are gathered by the program. Reading the velocities off Figure 4.1 lead to approximately 1845 m/s. This is a reasonable result comparing the calculated Gurney constant of 3.03 km/s (LX-14) with the reference values of Section 2.6.2 ($\sqrt{2E}_{\text{LX-14}} \approx 2.80 - -2.96$ km/s) even though the Gurney constant is higher than the referenced values. As a consequence, there is no need to change the method of attaining velocity values for this calculation.

However, the use of moving gauges turned out to be problematic when increasing the mass of the cylinder, i.e., M/C $>$ 2.2. The higher the values of M/C the more impractical becomes an array of moving gauges. This will be explained in the following. The Y-velocity of moving gauges for another cylinder configuration is shown in Figure 4.2. Now the cylinder has a mass nine times the mass of the charge, i.e., M/C = 9. This ratio is the only parameter that was changed. The positions of the gauges as well as the way of initiating the charge are the same as before. With this course of velocities it is impossible to read off an exact value.

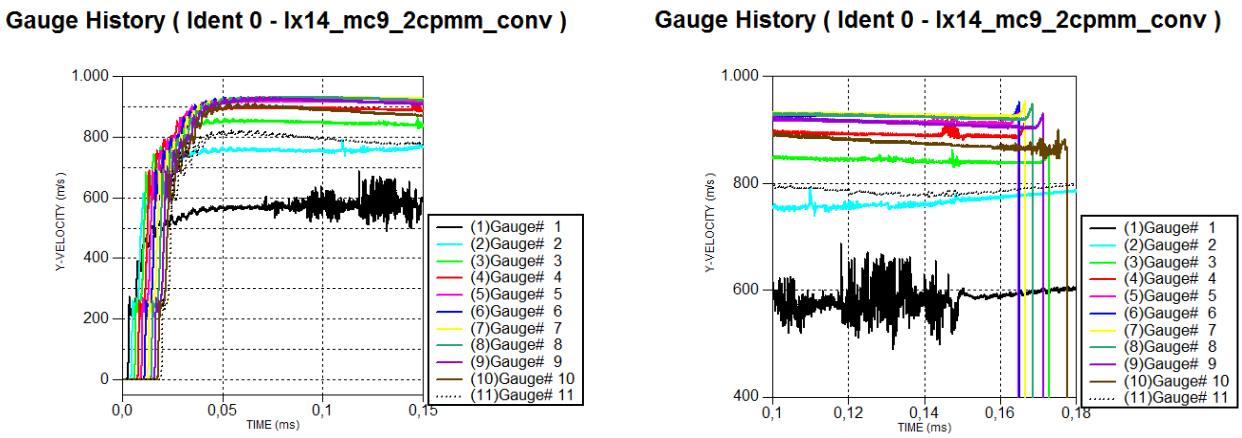


Figure 4.2: Y-velocity of the moving gauges of a 5 cm charge of LX-14 with an increased cylinder wall thickness, M/C = 9, circumferential initiation points.

Gauge number seven reaches over 920 m/s, whereas the asymptotic velocity of gauge number ten is 868 m/s. Gauge number two only reaches 780 m/s. With these very differing values the result can only be used to get an idea of the exact final velocity of the cylinder wall. On one side, averaging the final velocity of the gauges would certainly not be the real final velocity of the cylinder wall regarding experiments. On the other side, declaring the final velocity of one arbitrarily chosen gauge as the final velocity of the cylinder wall would neither be a suitable solution. However, not only increasing the M/C ratio leads to problems concerning moving gauges. Reducing M/C to values below 2.0 could cause problems as well. With a cylinder wall that thin, it begins to fracture early, so it is possible that the gauges get influenced by turbulences caused by the surrounding explosive.

In summary, measuring velocities with moving gauges does not result in reliable, accurate results. This problem is amplified as the cylinder wall increases, as shown in Figure 4.1. For that reason, fixed gauges were used in addition. A Y-array of fixed gauges was arranged at the middle of the cylinder length. The first gauge was arranged with a distance of 2 mm from the cylinder wall. Every 2 mm another gauge was implemented. Therefore, the exact XY positions of all gauges are known. AUTODYN provides a number of variables, so there are several options to measure a velocity with fixed gauges.

**pressure** As soon as the cylinder begins to expand and moves through the fixed gauges they show an increase of pressure. Due to the variation of the maximum pressure in time the results are not always as clear as assumed.

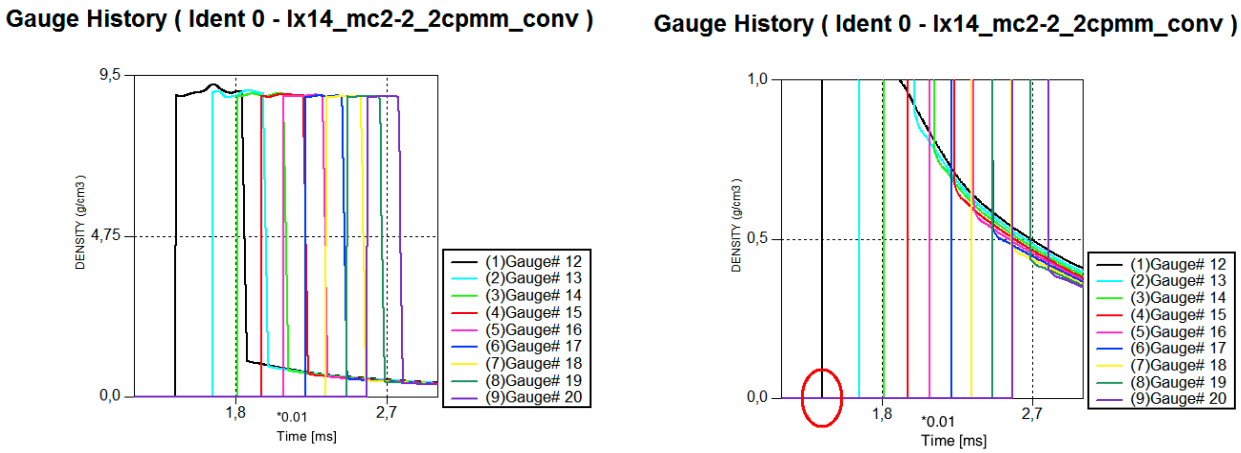


Figure 4.3: Density of the fixed gauges over time

**Y-velocity** The moment the cylinder passes one gauge, it detects a Y-velocity, whereas before there was no motion.

**density** Initially VOID fills out the whole part. The density of this surrounding is zero. Copper, by contrast, has a density of 8.93 $g/cm^3$. That leads to a significant increase in the chart of density vs. time once copper reaches a gauge.

Every method described has been tested, showing that most of the results were not as clear as theory indicates. Concerning pressure for example, it turned out that the maximum pressure is not always measured by gauges as soon as the cylinder wall passes the gauge. In some cases, the maximum pressure occurs just after the copper wall passes or even before. This may be caused by the detonating charge. Therefore it is impossible to determine the time the cylinder wall passes a gauge for each gauge equally by using the time of maximum pressure. The same problem occurred by using the maximum Y-velocity as a variable to investigate the motion of the cylinder wall. The only reliable method of detecting wall impact against a fixed gauge was density change, which is abrupt. In order to calculate a velocity, a distance vs. time graph has to be manually drawn up whereas the measured points are gathered from the density vs. time history shown in AUTODYN. For an assortment of gauges, the density vs. time chart is shown in Figure 4.3. Gauge 12 is the first gauge of the column, hence, the nearest to the cylinder wall. The other gauges follow in 2 mm steps. In order to identify the exact moment of time when the copper passes a gauge, the scale has to be enlarged. By clicking on the course of density in the area of the ellipse, the time can be read off. As the position of each gauge is known, a diagram

of distance vs. time can be prepared, which is illustrated in Figure 4.4.

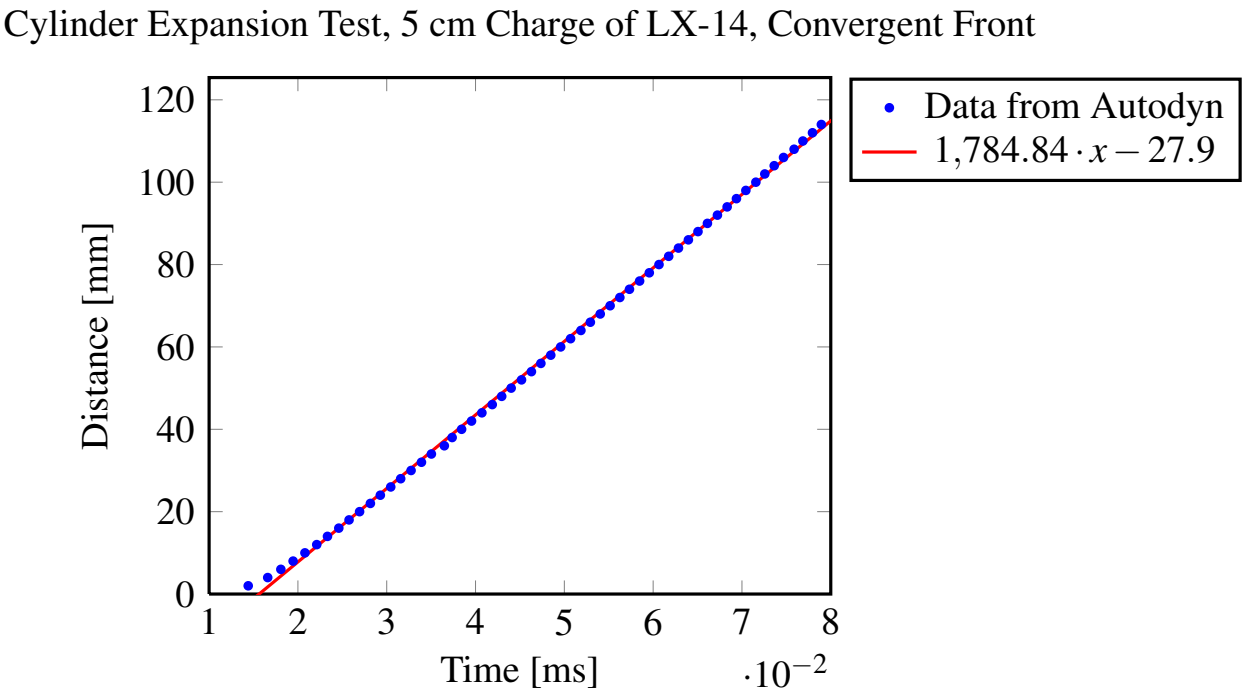


Figure 4.4: Distance vs. time data gained from pressure history

By adding a trendline through these experimentally gained measure points, the velocity of the cylinder wall can be read out of the chart. The slope of the trendline shown in Figure 4.4 corresponds to the final velocity. In this case it is 1784.84 m/s. The velocity predicted by the moving gauges was 1845 m/s (see Figure 4.1). The reason is that early velocities of the cylinder (in the first decimeter of expansion) are included in the calculation of the final velocity. The distance vs. time graph starts at a distance of 2 mm. The acceleration of the cylinder is not yet finished, so the velocity increases afterwards. This might lead to lower final velocities, respectively lower Gurney constants, than in real experiments, but allows for comparable simulations. In fact, taking into account only the last 20 mm of expansion of the same configuration as in Figure 4.4, the velocity is higher, as shown in Figure 4.5. The slope of the trendline is now 1854.98 m/s, which illustrates the ongoing velocity increase of the cylinder wall. This examples shows, that there is an uncertainty in the calculation of the velocity. It is not yet clear, whether the final velocity is measured with this technique.

**Uncertainty of Measurement**

The measured final velocity depends on the technique of measurement. Moving gauges determine other velocities than fixed gauges and concerning fixed gauges, their number respectively the length of radial expansion they cover is important. Taking into account the whole way of expansion as in Figure 4.4 leads to final velocity of 1785 m/s. Figure 4.5 displays 1855 m/s for the last 20 mm of expansion. This is a variance of almost 4%. Considering only the last 10 mm of expansion leads to a velocity of 1826 m/s which results in approximately 2% variance. An uncertainty of 2–4% results in a variance of up to 0.1 km/s for the Gurney constant and up to 70 m/s regarding final cylinder wall velocities.

Therefore, this uncertainty has to be considered while comparing results in this work. This fact might lead to minor differences in Gurney constants or even equal Gurney constants, although they seem to be different at first. The results of resolution and size, which are presented in the next section are a good example. Referring to Table 4.1 and Table 4.2 in advance, these Gurney constants might be all equal. This problem only refers to the cylinder expansion test simulation series. For the simulations of the Andrews experiment, the reference data is documented in Andrews' report.

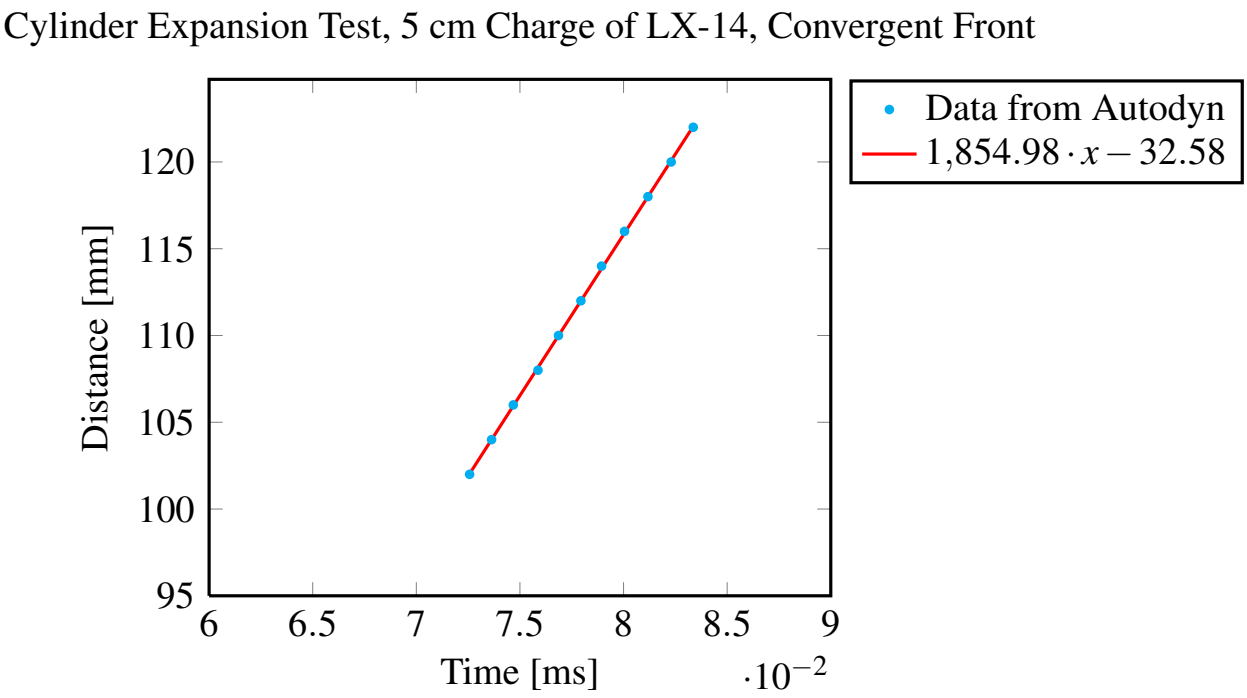


Figure 4.5: Distance vs. time data for the last 20 mm of expansion that were measured

## 4.2 Problems of Size and Resolution

Concerning numerical problems, size and resolution are always important issues. On one side the goal is to gain information and results as exact as possible, which requires a fine mesh of the computational model and therefore a high resolution.

On the other side, the resolution has to be as low as possible in order to save computing time. The more cells the model consists of, the more cells have to be computed. Changing the resolution from two cells per millimeter to four cells per millimeter results in four times more cells. In order to examine the effect of resolution, a certain setup was calculated in three different resolutions. A two cells per millimeter, a four cells per millimeter and finally a six cells per millimeter resolution. The considered model was a 5 cm charge of LX-14, filled in a copper cylinder and initiated by a single detonation point. The M/C ratio was 2.2. According to this model, 238,000 cells have to be computed at first. A resolution twice as accurate leads to a total number of 952,000 cells and the highest resolution contains 2,142,000 cells as a consequence of the refined mesh. With respect to the used hardware, the two cell per millimeter simulation was calculated in less than an hour, whereas the six cell per millimeter resolution took four days to be calculated. Thus, the challenge is finding a compromise between predictive accuracy and computing time. Considering numerical solutions, which implies an approximation of the theoretically exact result, rounding errors are an issue. This feature has to be kept in mind while refining the mesh. The more cells there are, the more important becomes the problem of rounding errors. This problem is not further considered in this work, however, it is an inevitable feature. The results of the calculations with the different resolutions are listed in Table 4.1.

Table 4.1: Results of the study of resolution for a 5 cm charge LX-14, point initiated

| Resolution in Cells per Millimeter | Total Number of Cells | Wall Velocity [m/s] | Gurney Constant [km/s] | Approx. Calculating Time |
|---|---|---|---|---|
| 2 | 238,000 | 1778 | 2.92 | $<$1hour |
| 4 | 952,000 | 1758 | 2.89 | 36 hours |
| 6 | 2,142,000 | 1756 | 2.88 | 4 days |

The number of cells, the final wall velocity of the cylinder, the Gurney constant and the real calculating time of the three different resolutions are listed. Regarding the calculating time, it has to be stated that this is heavily dependent on the utilized hardware. The values of this column just describe the results of the computer used in this work[6].

[6]HP DL580 G7 E7, High Performance - Server, 4 x Xeon E7-4870,10 cores each, 2.4 GHz - RAM 512 GB

As a first observation, it can be stated, that all results are in the same dimension and no value differs tremendously. However, there is a trend concerning the velocities and Gurney constants. The higher the resolution is, the lower the final velocities are. Although there is almost no difference between the four and six cells per millimeter resolution, there is a slight difference to the lowest resolution. In general it can be stated that the calculated Gurney constants do not deviate much from the value of 2.80 km/s, which is an experimentally gathered reference value for LX-14 listed in Table 2.5. Calculated estimates for LX-14 differ from 2.66 km/s to 2.96 km/s, as listed in Table 2.4. However, taking into account the number of cells, respectively the computing time and the consequential results, the lowest resolution is recommended for simulation series of this work. Despite these results, the recommended resolution of the mesh depends on the required accuracy of results and availability of hardware and time.

Another variable, which has to be considered in numerical simulations, is the size of the model. According to Gurney, $\sqrt{2E}$ is a material constant and, correspondent to Equation 2.7, theoretically independent of the size of the model. However, there is an effect of scaling in practice, which has to be examined in numerical simulations. Therefore, a scaled cylinder was set up. Each length was multiplied by three. As a consequence, the cylinder was now 915 mm long, had a diameter of 150 mm and the cylinder wall was 15.4 mm thick. Initiated by a single detonation point, the model was implemented with a two cell per millimeter resolution. The results of this simulation were compared to the results of the 5 cm charge with the same resolution, mentioned above. A comparison of the two sizes is listed in Table 4.2.

Table 4.2: Results of the study of size for LX-14, point initiated

| Charge Diameter | Total Number of Cells | Wall Velocity [m/s] | Gurney Constant [km/s] | Approx. Calculating Time |
|---|---|---|---|---|
| 5 cm | 238,000 | 1778 | 2.92 | $<$1hour |
| 15 cm | 1,047,200 | 1763 | 2.89 | 10 hours |

Again, a trend to lower velocities and Gurney constants can be observed. Regarding the simulation itself, it is to state that a relatively large amount of energy seems not to be able to impart an effect on the cylinder wall velocity. Due to the enlarged diameter of the cylinder, the detonation gases move directly out of the end of the cylinder where the initiation starts, without being part of the metal acceleration, especially concerning the first quarter of the cylinder. In this work, cylex tests with various M/C ratios were done for both the 5 cm and the 15 cm charge. Further results can be found in Section 5.2.2. However, the derivation of the calculated Gurney constant

are very low. Considering the possibly contained uncertainty of up to 0.1 km/s for the Gurney constant, there do not have to be a difference in resolution and size at all.

## 4.3 Detonation Initiation

There are different ways of initiating an explosive in AUTODYN. In this work, each explosive was modeled with the Jones-Wilkins-Lee (JWL) equation of state and only detonation points were applied. The different detonations paths as well as possible implementations of convergence are described below.

### 4.3.1 Direct vs. Indirect Detonation Path

When implementing detonation points in AUTODYN, there is a choice between direct and indirect detonation path. The main difference is the treatment of inert material in the direct path of the moving detonation front. Using direct path, AUTODYN computes the detonation front along a straight line from the point of detonation to each cell center, regardless of material regions [4]. This is the most accurate method as long as the paths goes through explosive material. Selecting indirect path, AUTODYN computes automatically the shortest paths through explosive and around inert material [24]. The different shapes of the detonation waves are illustrated in Figure 4.6. The direct path does not reckon in the inert material, so the detonation wave moves through the material as it would all be explosive. On the contrary, the indirect detonation path calculates the path of detonation around the inert material of the part.

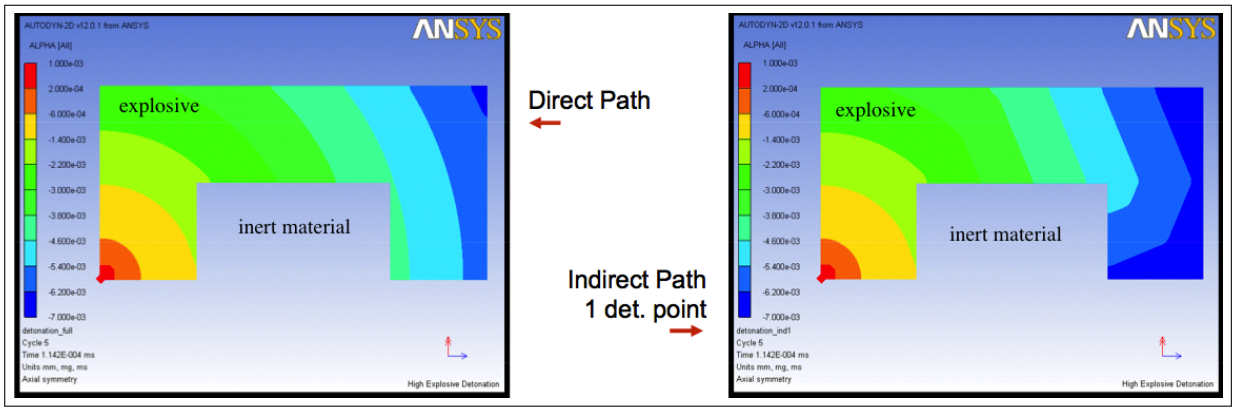


Figure 4.6: Difference between direct and indirect detonation paths [4]

Most calculations of this work were initialized with a direct path due to the absence of inert material in way of the detonation front in cylinders. The indirect path was applied to calculations with cylinders containing two explosives such as the Andrew configuration due to possible

interactions at the interface. A preliminary series of calculations comparing results of direct and indirect detonation point initiation showed a minor difference regarding only one explosive material. The final wall velocities of the cylinder filled with LX-14 are listed in Table 4.3. Since only one calculation per mass ratio and detonation configuration was computed, a statistical evaluation cannot be given here. However, the largest occurred variation is approximately 2.5% for the point initiation and 1.5% for the convergent front configuration as shown in Table 4.3.

Table 4.3: Variation in velocities of cylinder expansion tests as a result of direct in comparison to indirect detonation paths for a 5 cm charge of LX-14

| M/C | Point Initiation | | | Convergent Front | | |
|---|---|---|---|---|---|---|
| | $v_{direct}$ [m/s] | $v_{indirect}$ [m/s] | Variation [m/s] | $v_{direct}$ [m/s] | $v_{indirect}$ [m/s] | Variation [m/s] |
| 1 | 2480 | 2485 | -5 | 2683 | 2642 | 41 |
| 2.2 | 1780 | 1792 | -12 | 1803 | 1809 | -6 |
| 3 | 1545 | 1547 | -2 | 1531 | 1547 | -16 |
| 5 | 1208 | 1195 | 13 | 1213 | 1214 | -1 |
| 7 | 1003 | 996 | 7 | 1032 | 1025 | 7 |
| 9 | 865 | 856 | 9 | 895 | 890 | 5 |
| 10 | 824 | 803 | 21 | 845 | 846 | -1 |

### 4.3.2 Implementation of Convergence

For this work, two different methods of implementing a convergent front were deployed. As mentioned in the technical issues, Andrews used a composite of two explosives to create a convergent front. However, there is the possibility to implement a convergent detonation front by setting a circumferential X-array of single detonation points in the explosive, right below the cylinder wall. The initiation time of each point can be set separately. Goal is an initiation sweep rate higher than the detonation velocity of the explosive. As shown in Table 2 in the Appendix, the detonation velocity of LX-14 is 8.8 km/s, TNT detonates with 6.93 km/s and HMX is similar to LX-14 with a detonation velocity of 9.11 km/s. The initiation sweep rate was set to approximately 15 km/s. The sweep rate is not the only variable to determine. In a preliminary simulation series of this work, the quantity of detonation points respectively the distance between these points was varied in order to detect possible variations of results. Arrays of 15, 30 and 61 detonation points were compared. A distance of 20 mm between the detonation points, which results in 15 detonation points, is too far to generate an even detonation front. Due to the manual entering of initiation times, an array of 61 detonation points (spacing of 5 mm) is

not recommended, although it results in a steady detonation front. The best solution is an array with 30 points, respectively 10 mm spacing. The XY coordinates of the first detonation point are (5,25). All calculations concerning the parameter study of the cylinder expansion test were computed with a 10 mm gap between the detonation points.

On the other hand there is the option of realizing a convergent detonation front by filling the cylinder with two explosives with different detonation velocities, just as Andrews did. Certainly, the one with the lower detonation velocity depicts the core. In order to initiate both explosives at the same time, a booster charge is arranged ahead of the cylinder. Once the booster is initiated by a single detonation point, the detonation wave travels towards the cylinder and initiates both the sleeve and the core explosive almost at the same time. Due to the higher detonation velocity of the sleeve, which overdrives the core explosive, a convergent detonation front occurs.

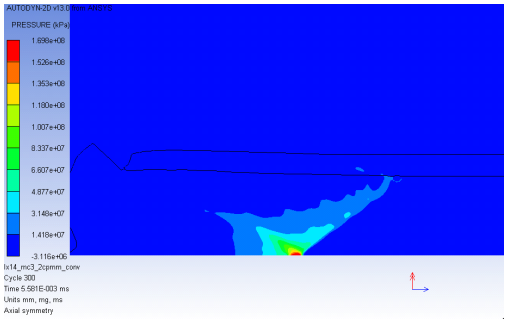


Figure 4.7: Convergence through circumferential detonation points

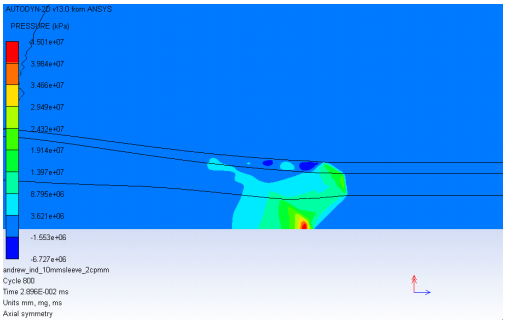


Figure 4.8: Convergence by using two explosives

The two methods of implementing a convergent front are shown in Figure 4.7 and Figure 4.8. The high pressure peak at the center of the front and the different detonation velocities of the sleeve and the core are illustrated. As a matter of fact, the detonation front in the sleeve is planar. There is an obvious bend in the shape of the detonation front comparing the sleeve with the core explosive. Due to the adjustable scale of both captures, the contours visualizing the pressure cannot be compared. The detonation points are not displayed in order to focus on the shape of the detonation front.

## 4.4 Model Setup

The exact model configuration in ANSYS AUTODYN is shown by the 5 cm cylinder expansion test model. To show one method of implementing a convergent detonation front, this example is initiated by an array of circumferential detonation points. The model is shown in Figure 4.9.

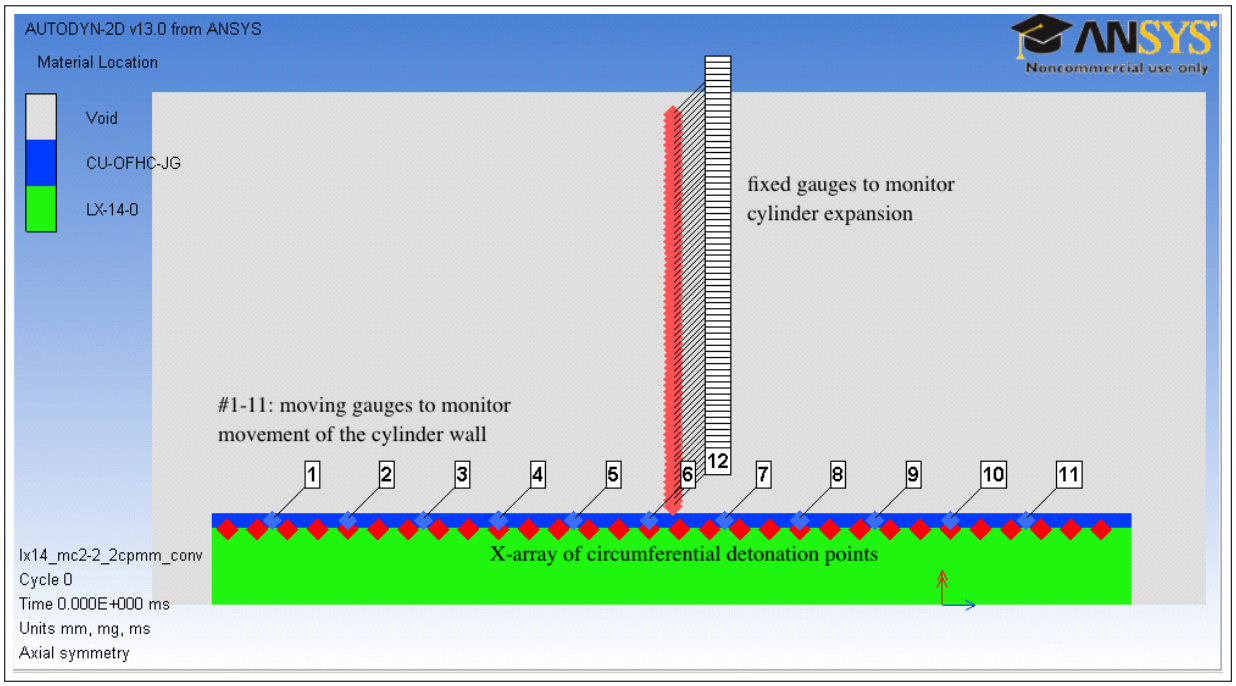


Figure 4.9: Model of the cylinder expansion test initiated by circumferential detonation points

1. **New setup**
   In order to start a new model, a name must be provided as well as the dimension of the model (2D or 3D) and the units AUTODYN should use to give out the results. All models for this research were set up as axially symmetrical 2D models. Calculations were done in mm, mg and ms. The units have to be checked in order to interpret the results correctly.
2. **Materials**
   Materials can either be chosen from the AUTODYN library or newly defined. Every used material is listed in the Appendix. PBXN-111 and PBXN-110 are not in the library, so they have to be defined with the parameters listed in Table 3 of the Appendix. Furthermore, materials can be modified for the purpose of special use which was applied to "Steel 1006" in this research.

3. **Boundaries**

   To create a new boundary, name and type have to be selected. For this work a "Flow_Out" boundary with the standard sub option "Flow out (Euler)" was determined. Choose "EQUALL ALL" in the tab of Preferred Materials in order to allow materials to flow out through the edges of the model. A "Transmit" boundary can also be used as seen in some other works concerning detonation problems [25, 26]. However, this is not recommended because a "Transmit" boundary only transmits the perpendicular component, while for blast simulations in Euler the "Outflow" boundary is recommended [27].

4. **Parts**

   To create a part its coordinates have to be set and the optimal problem solver has to be chosen. Detonation simulations are usually set up with the Euler solver to use a fixed mesh and therefore avoid little timesteps generated by deformed Lagrange parts. In this case, a rectangular Euler part was designed with the part wizard. The standard cylinder for these kind of experiments is 305 mm long, so the X-coordinates of the part were set as $X = -10$ and $DX = 350$ (mm). To allow appropriate observation of the cylinder expansion, the Y-coordinates were set as $Y = 0$ and $DY = 170$. An important factor of a numerical calculation is the resolution of the model. This problem is explained in more detail in Section 4.2. For a two cell per millimeter resolution set $I = 700$ and $J = 340$. For further comprehension it has to be said that the XY coordinates refer to the geometrical coordinates of the whole part, as opposed to the IJ coordinates which refer to the cells. Therefore, XY coordinates can be negative whereas IJ coordinates are always positive and start with 1 as the first value. The final step is filling the part with VOID. If a special part of the model needs closer consideration the mesh can be zoned to get a more detailed resolution in the part of interest. This method was not necessary in this work.

   (a) **Fill the Part**

   To refer material to the cells the part has to be filled. On one side there is the option to "Fill by Index Space" where material can be filled in the cells by IJ coordinates. Alternatively, there is the option to "Fill by Geometrical Space" where XY coordinates are used to fill the part and therefore the material is not fixed with the cell mesh. Hence it is possible to fill the parts in fractions of a millimeter even if the mesh is set to one cell per millimeter. It turned out that the method of filling by geometrical space is much more appropriate for this work. At the beginning of this research the "Fill by Index Space" method was used to set up the model. Apparently, this method needed more computation time even with a one cell per millimeter res-

olution. A two cell per millimeter resolution was almost impossible to compute. Another disadvantage is that the option of zoning cannot be used properly with this method because the material is connected to the cells rather than to fixed coordinates. Regardless of the difference of these methods concerning computer code, it is important to note that the "Fill by Geometrical Space" option is the one preferred. For the cylinder expansion test the rectangular fill can always be used according to the simple geometry of the model.

(b) **Gauges**

Either fixed or moving gauges can be arranged in AUTODYN and there is again the choice between IJ coordinates and XY coordinates, whereas the latter were chosen for this work. To measure the velocity of the cylinder wall, both an X-array of moving gauges and a Y-array of fixed gauges were arranged in the model. In some calculations the detonation velocity is a matter of interest so another X-array of fixed gauges was arranged in the explosive. In order to measure the velocity of the steel disk concerning the disk launch calculations, more X-arrays of fixed gauges were set behind the disk along the axis and above. The exact use of the gauges to measure all interesting velocities is explained in section 4.1.

(c) **Boundaries**

The boundary has to be adapted to the existing part. In order to allow all materials to flow out of the part where it is necessary, two I-lines as well as a J-line have to be set. In this example the boundary is applied to the lines I=1, I=351 and J=171, which conforms to the upper edge of the part as well as both sides.

5. **Detonation**

For this setup the convergent detonation front was accomplished by a Y-array of single detonation points in the explosive near the cylinder wall. The sweep rate of the circumferential initiation of these points has to be set up manually by setting the initiation time. For a point initiation a single detonation point with a direct detonation path can be set at the origin of the XY coordinates. To realize a planar detonation front either a detonation line or an array of single detonation points can be arranged.

6. **Controls**

AUTODYN will stop and give warning if energy error exceeds Energy fraction (default 5%). To avoid an early termination, set the Cycle and Time limit really high, e.g., 9999999. The Energy reference cycle also has to be set high to prevent AUTODYN from always checking on the energy balance and stopping the calculation as soon as energy

error exceeds Energy fraction. Additionally select "Internal" for the ALE/Euler Energy under the tab Transport.

7. **Output**

   This section contains every kind of output of the simulations. What a useful increment of saved cycles is depends on how many cycles a calculation will run. Concerning detonation problems, the data should be saved at least every 200 cycles. A refresh of the screen every 25 cycles is set by default. This value might be increased due to the additional time it takes to calculate all necessary parameters for refreshing the result of the current cycle. Additionally, the option of capturing images every specified cycles can be selected.

8. **Plots**

   This is the choice of how the calculation should be illustrated. Choose from one of the fill types material location, material status or contour, whereas the variable of the contour can be selected. In order to make detonation fronts visible, set pressure as the variable of the contour fill type. Additional components such as vector, detonation points, gauges, boundaries, axis or the grid can be added to the current plot. This a good way to check whether these components were set correctly. Although a 2D model is used for calculations, a 3D view can be generated by rotating the model along the axis.

9. **Further recommendations**

   As soon as the Run button is clicked, AUTODYN initiates the model and starts to calculate. It is highly recommended to stop the simulation directly in order to decrease the minimum timestep. Go back to Controls and set the minimum timestep to at least $10^{-10}$ to avoid an early termination. This cannot be done until the simulation was started once.

THIS PAGE INTENTIONALLY LEFT BLANK

# CHAPTER 5:
# Results of the Research

Results of all simulations are reported in this chapter. At first, results of preliminary simulations are presented. These include mainly comparisons between different methods of implementing initiation. The preliminary simulation results are followed by the results of the cylinder expansion tests. Focus of this series is the modification of the M/C ratio and the effects on Gurney. At the end, the simulations of the experiments conducted by Andrews et al. [1] are analyzed.

## 5.1 Preliminary Simulations

In order to be able to understand the differences in initiation which are provided by ANSYS AUTODYN, data was gathered during a preliminary simulation series. Obtaining awareness of the various settings by comparing different counts of detonation points in an array was used to determine a consistent method, which was thereafter used for every simulation. Earlier in this work a planar front was realized by an Y-array of detonation points. Later, only a single detonation point was used. Different counts of these points had been compared to the implementation of a detonation line.

### 5.1.1 Quantity of Detonation Points

For the cylinder expansion test simulations, the convergent front was realized by an X-array of circumferential detonation points. Earlier in this research, the quantity of these detonation points had been modified as already mentioned in Section 4.3.2. Simulations had been done with an array of 15 detonation points, respectively 20 mm distance between the points, an array of 30 points with a 10 mm gap in between, and with an array of 61 detonation points, which leads to a 5 mm gap between these points. The sweep rate of these points was always the same and set to 15 km/s. Subject of this scrutiny was a cylinder expansion test with a 5 cm charge of LX-14. Due to the early state of this research in which these simulation were done, the model was built with the "Fill by Index Space" method and a resolution of just one cell per millimeter. Besides, the final velocity was measured exclusively with moving gauges. That leads to the recommendation of not taking the following Gurney constants, calculated with the data of these simulations, as absolute values. They would rather be proper for comparing the results of these preliminary simulations among one another. The results of this simulations series are listed in

Table 5.1. The Gurney constants for the three different counts of detonation points for several M/C ratios each are displayed.

Table 5.1: Cylex test with 5 cm charge LX-14: Gurney constants for initiation by arrays of different counts of detonation points

| M/C ratio | $\sqrt{2E}$ [km/s] for 15 detonation points | 30 | 61 | Average $\sqrt{2E}$ [km/s] | Variance from Average for 15 detonation points [%] | 30 | 61 |
|---|---|---|---|---|---|---|---|
| 1.0 | 3.11 | 3.12 | 3.12 | 3.12 | 0.32 | 0.00 | 0.00 |
| 3.0 | 3.02 | 3.01 | 2.99 | 3.01 | -0.33 | 0.00 | 0.66 |
| 5.0 | 3.02 | 3.02 | 3.00 | 3.01 | -0.33 | -0.33 | 0.33 |
| 7.0 | 3.07 | 3.06 | 3.06 | 3.06 | -0.33 | 0.00 | 0.00 |
| 9.0 | 3.11 | 3.10 | 3.08 | 3.10 | -0.33 | 0.00 | 0.65 |
| 10.0 | 3.10 | 3.10 | 3.09 | 3.10 | 0.00 | 0.00 | 0.32 |

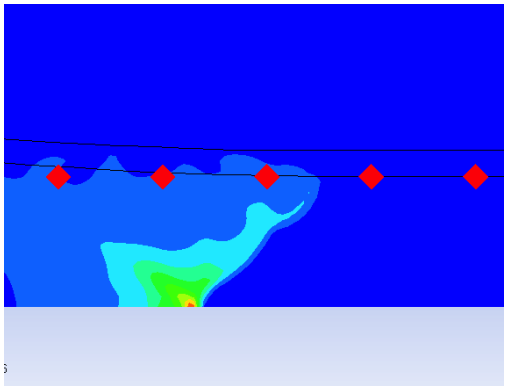

Figure 5.1: Detonation front evolved from 15 detonation points

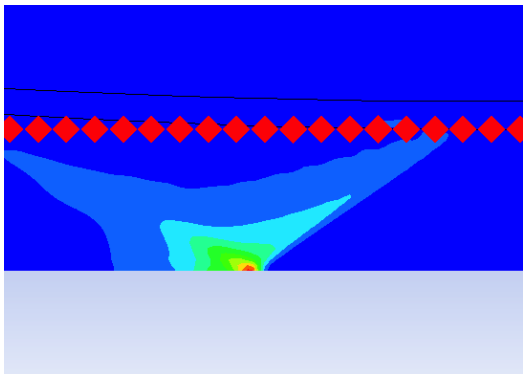

Figure 5.2: Detonation front evolved from 61 detonation points

The three values for each M/C ratio were averaged and the variance of each value from this average was calculated. There is no significant difference in results between the implementation of 15, 30 or 61 detonation points. The variance mostly is $\pm 0.3\%$. Based on the slightly differing calculated Gurney constants, there is no general recommendation for one, respectively against one specific configuration. However, 15 detonation points seem to be too few to develop a steady detonation front. Detonation fronts of the configuration of 15 points and the configuration of 61 points are compared in Figure 5.1 and Figure 5.2. Due to the varying scale, the colors representing the pressure cannot be compared. These Figures just show the difference in shape

of the detonation front. The position of the detonation points and their initiation time have to be set manually. Therefore, the implementation of 61 detonation points was not found to be useful in this work. Hence, an array of 30 detonation points was used for all further simulations.

It is noticeable that the averaged Gurney constants of Table 5.1 (3.01–3.10 km/s) are higher than the experimentally gathered values of Table 2.5 (2.80 km/s) and the predicted values of Table 2.4 (2.66–2.96 km/s).

### 5.1.2 Detonation Line vs. Detonation Points

In order to realize a divergent, planar front there are also a number of possibilities concerning the placing of detonation points. In further calculations only one single detonation point was placed on the center line of the explosive. In this early stage of research, methods of implementing an array of six (5 mm gap in between), respectively 13 detonation points (2 mm gap in between) were compared to the implementation of a vertical detonation line. The implementation of an Y-array of six detonation points is shown in Figure 5.3 and Figure 5.4 illustrates the implementation of the detonation line. These Figures show an excerpt of the model for a cylinder expansion test. As mentioned before, the model for this simulation series was also set up with the "Fill by Index Space" method and with a resolution of one cell per millimeter. Furthermore, only moving gauges were used to measure the velocity.

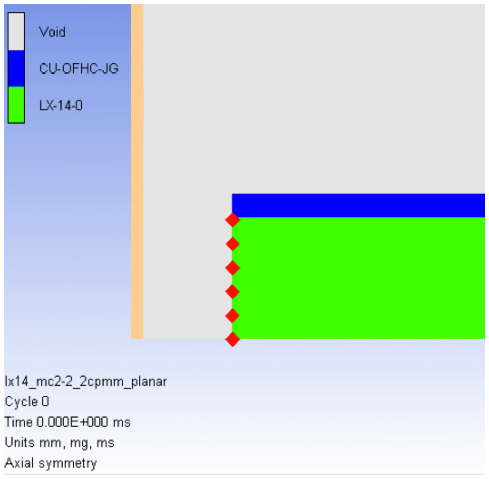


Figure 5.3: Implementation of a Y-array

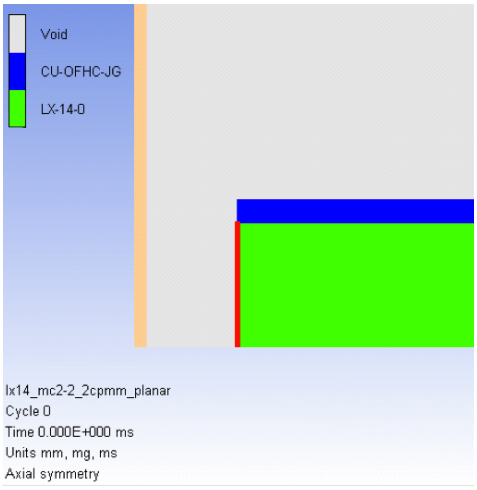


Figure 5.4: Implementation of a detonation line

Therefore, the calculated values of Gurney constant should just be used to compare the simulations of this series among one another. Table 5.2 contains the calculated Gurney constants in km/s of each configuration for a number of M/C ratios. The average and the variance of each calculated Gurney constant from this average also are listed. None of the investigated configurations presents remarkable variation. Variances are in the range of $\pm 0.98\%$. Due to the fact that only one simulation was done for each set of parameter, no further statistical analysis is possible. In summary it can be stated that there is no major difference in implementing a planar front by Y-arrays of different counts of detonation points or by a vertical detonation line.

Table 5.2: Cylex test with 5 cm charge LX-14: Gurney constants regarding initiation by detonation points vs. a detonation line

| M/C ratio | $\sqrt{2E}$ [km/s] for 6 detonation points | $\sqrt{2E}$ [km/s] for 13 detonation points | $\sqrt{2E}$ [km/s] for detonation line | Average $\sqrt{2E}$ [km/s] | Variance from Average for 6 points [%] | 13 points [%] | line [%] |
|---|---|---|---|---|---|---|---|
| 1.0 | 3.07 | 3.04 | 3.07 | 3.06 | -0.33 | 0.65 | -0.33 |
| 3.0 | 3.00 | 2.99 | 3.01 | 3.00 | 0.00 | 0.33 | -0.33 |
| 5.0 | 3.02 | 3.02 | 3.02 | 3.02 | 0.00 | 0.00 | 0.00 |
| 7.0 | 3.03 | 3.03 | 3.03 | 3.03 | 0.00 | 0.00 | 0.00 |
| 9.0 | 3.10 | 3.07 | 3.04 | 3.07 | -0.98 | 0.00 | 0.98 |
| 10.0 | 3.07 | 3.06 | 3.04 | 3.06 | -0.33 | 0.00 | 0.065 |

Here, too the averaged Gurney constants of Table 5.2 (3.00–3.07 km/s) are higher than the experimentally gathered values of Table 2.5 (2.80 km/s) and the predicted values of Table 2.4 (2.66–2.96 km/s).

### 5.1.3 Target Deformation

In order to observe the deformation of a steel disk that was put at the end of a cylinder filled with explosive, a number of preliminary simulations were calculated with an unmodified steel disk. For the Andrews experiment, the yield stress of the steel disk was increased to avoid deformation. Subject of this simulation series were the deformations caused by a planar front on one side compared to deformations caused by a convergent front on the other side. The results for the planar front are shown in Figure 5.5 and Figure 5.6 illustrated the results for the convergent front. In order to avoid cylinder expansion, steel was used for the cylinder walls, which were thickened up. The figures were captured at almost the same time regarding real time. The pressure throughout the planar detonation front is constant, therefore, it impinges on the steel disk at its whole surface evenly.

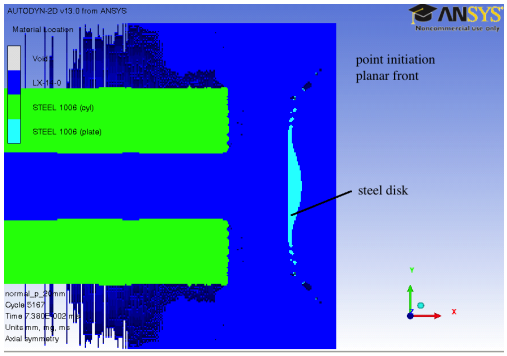


Figure 5.5: Deformation caused by a divergent front

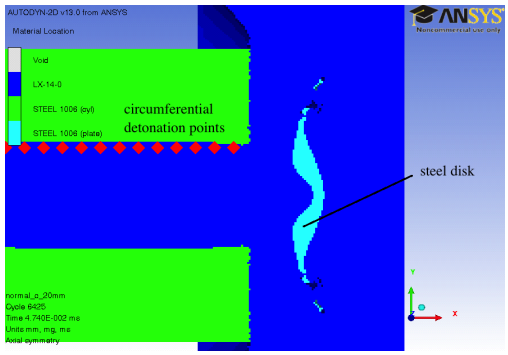


Figure 5.6: Deformation caused by a convergent front

That leads to an immediate acceleration of the whole disk. On the contrary, the convergent front has no steady pressure profile along its front. The maximum pressure is found at the center line of the front. Due to its geometry, the convergent front impinges at first upon the steel disk at its upper and lower edge but with a lower pressure compared to the planar front. Tremendous deformation is then caused as soon as the high pressure peak of the convergent front along the center line of the cylinder dashes against the disk. Depending on charge diameter and disk thickness, it is possible to shatter the disk. A convergent front causes more deformation whereas a planar front achieves more displacement of the disk. Concerning the convergent front, there is much gas leakage and therefore a loss of energy, which cannot be used to accelerate the disk, because the detonation products escape through the gaps at the lower and upper edge of disk that emerge as soon as the front impinges upon these edges of the disk and starts to deform it.

### 5.1.4 Detonation Front Angle $\alpha$

In this work the cylinder expansion test was simulated with three different explosives. Convergent and planar fronts were compared for copper cylinders filled with LX-14, TNT and HMX. The angle of the emerged convergent front depends on the sweep rate of the circumferential initiation points and the detonation velocity of the examined explosive. Therefore, each explosive presents a different angle when initiated with the same sweep rate. The sweep rate in this work was set to approximately 15 km/s. The larger the difference between sweep rate and detonation velocity, the steeper is the angle of the front. Angle $\alpha$ was regarded as the angle between the detonation front and the cylinder axis (see Figure 5.7) and is listed in Table 5.3.

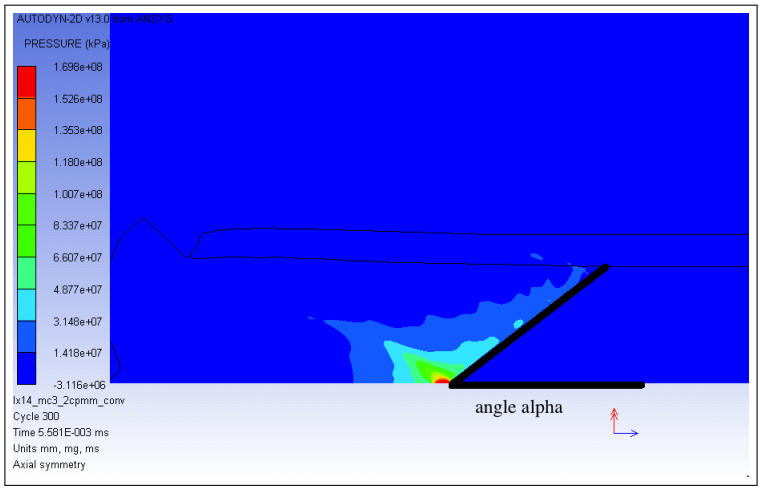


Figure 5.7: Illustration of the angle $\alpha$ concerning the shape of the convergent front.

Table 5.3: Angle $\alpha$ of the convergent front for each explosive with a sweep rate of 15 km/s

| Explosive | Detonation Velocity [km/s] | Angle $\alpha$ [degree] |
|---|---|---|
| HMX | 9.11 | 40° |
| LX-14 | 8.80 | 38° |
| TNT | 6.93 | 28° |

### 5.1.5 Effective Charge Calculations

As far as previous experimental results are concerned, only a part of the whole charge is effective in accelerating metal. For a cylindrical charge, the so called effective charge is a cone with a 60° base angle and the the same diameter as the charge. In order to check this by hydrocode simulations, a cylindrical charge of LX-14 with no casing had been set up. The initial length of charge was determined to be 305 mm, based on cylex test simulations. A steel disk was put at the end of the charge. The thickness of that disk was determined to be 10 mm, 20 mm and 30 mm.

Regarding the diameter of the charge (50.8 mm) the height of the effective cone had to be 43.3 mm. This means that charges of lengths over 43.3 mm would show no advantage in accelerating the steel disk over shorter charges. For this reason, the cylindrical charge had been truncated stepwise. Beginning from the initial length of 305 mm to a length of just 24 mm. The results are shown in Figure 5.8.

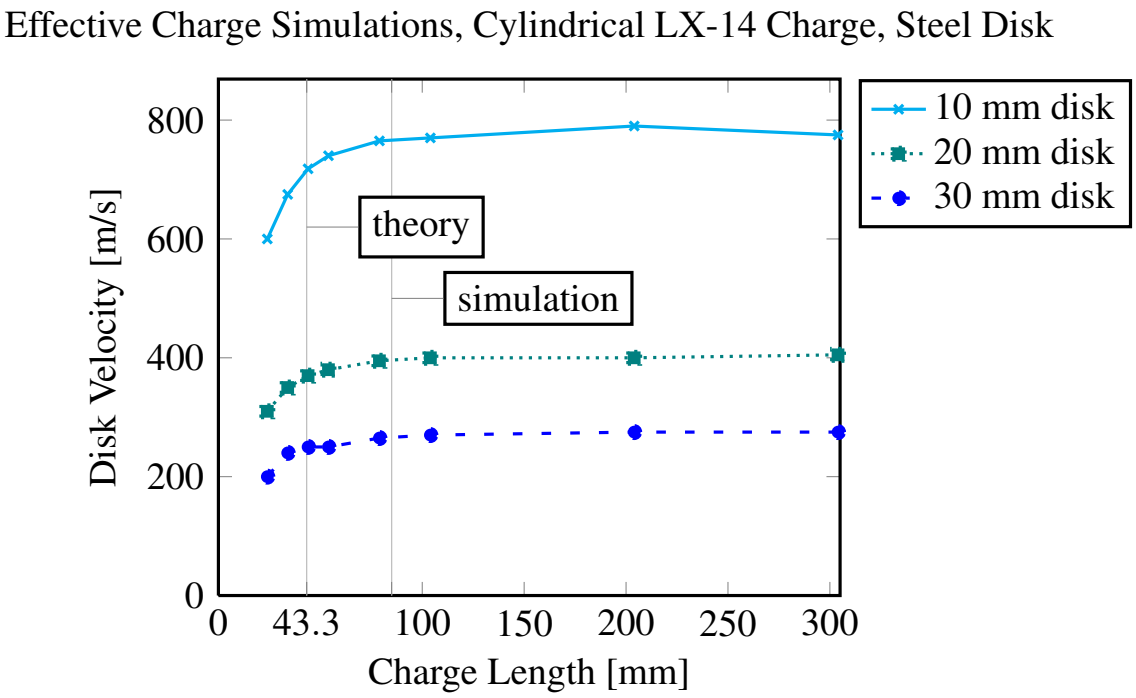


Figure 5.8: Results of the effective charge simulations for LX-14, planar front (6 detonation points)

According to theory, the velocity of the disk starts to decrease at a length of 43.3 mm, which is illustrated by an additional vertical line in the figure, marked as theory. The simulations were performed for three different disk thicknesses. The effective charge length of simulations had been found to be larger than the theoretical length. The second vertical line at approximately 90 mm and marked as simulations illustrates this result. The existence of an effective length of charge could be validated. However, the simulated length is not identical with the theoretical value. Further investigations especially of the charge lengths between 40 mm and 90 mm are recommended but could not be provided in this work. The model of the effective charge was checked in order to be able to calculate the theoretically possible final velocities of the steel disk that was put at the end of the cylinder in Andrews' experiment. Due to the existent copper cylinder of that configuration, the modified equation of Benham (see Section 2.4) had to be used. Further results of metal acceleration are listed in Section 5.3.2.

## 5.2 Validation of Cylinder Expansion Tests

In the context of this simulation series, the effect of convergence on cylinder expansion in regard to the Gurney constant was investigated. The 5 cm charge of LX-14, respectively TNT or HMX, was arranged in different M/C ratios in order to examine the effect of convergence and an increasing mass of the cylinder on Gurney constants. To verify the results for this charge, a 15 cm charge of LX-14 was also investigated over a number of M/C ratios.

### 5.2.1 Effect of Convergence on Cylinder Expansion

Goal of this research is to detect an effect of convergence on cylinder expansion, respectively the final wall velocity and therefore the Gurney constant. The results of the cylinder expansion test simulations with a 5 cm charge of LX-14, TNT or HMX are listed in Table 5.4. All these simulations were calculated with a resolution of two cells per millimeter and for a range of different M/C ratios. The final wall velocities and the derived Gurney constants are listed for the case of point initiation and the case of circumferential initiation points, which leads to a convergent front. The absolute differences are also listed. Regarding the differences between the Gurney constants of the planar front and the constants of the convergent front, there is no remarkable distinction. The values are all in the same range. This applies to all three explosives. From this, it can be inferred that there is no significant effect of convergence on cylinder expansion as far as these simulations are concerned. Furthermore, it can be stated that these calculated Gurney constant correspond well with the data calculated by estimates in Table 2.4.

### 5.2.2 Variation of M/C Ratio

In this section the focus was set on the dependence of the Gurney constant from the M/C ratio. Regarding the Gurney model and its equation, the Gurney energy is supposed to be a material constant and therefore independent of the M/C ratio. Ideally, the M/C ratio varies in the same matter as the final cylinder wall velocity so that this equation,

$$\sqrt{2E} = V\sqrt{\frac{M}{C}+\frac{1}{2}},$$

derived from the Gurney equation for the cylinder configuration, always returns the same value. As a matter of fact, a trend was found for the Gurney energy as a function of the M/C ratio. The Gurney constant vs. M/C ratio for both the point initiation and the convergent front are shown in Figure 5.9. First of all, these graphs show the slight difference in Gurney constants concerning the different methods of initiation.

Table 5.4: Results of the cylinder expansion test simulations for a 5 cm charge

| Explosive | M/C ratio | Final Velocity [m/s] | | | Gurney Constant [km/s] | | |
|---|---|---|---|---|---|---|---|
| | | point | convergent | difference | point | convergent | difference |
| LX-14 | 1.00 | 2461.7 | 2776.1 | 314.4 | 3.02 | 3.41 | 0.93 |
| | 2.20 | 1778 | 1778 | 0.2 | 2.92 | 2.92 | 0.00 |
| | 3.00 | 1530 | 1528 | 2.6 | 2.86 | 2.86 | 0.00 |
| | 5.02 | 1183 | 1198 | 14.7 | 2.78 | 2.81 | 0.03 |
| | 7.02 | 978 | 1010 | 31.87 | 2.68 | 2.77 | 0.09 |
| | 9.02 | 846 | 883 | 36.56 | 2.61 | 2.72 | 0.11 |
| LX-14 | average | | | | 2.81 | 2.92 | 0.11 |
| LX-14 | reference data | | | | 2.80 km/s [19] | | |
| TNT | 1.0 | 1989.1 | 2133.1 | 144 | 2.43 | 2.60 | 0.18 |
| | 2.47 | 1343 | 1346 | 2.3 | 2.32 | 2.32 | 0.00 |
| | 3.00 | 1233 | 1223 | 9.3 | 2.31 | 2.29 | 0.02 |
| | 4.98 | 945 | 954 | 9.2 | 2.21 | 2.23 | 0.02 |
| | 6.98 | 776 | 801 | 24.63 | 2.12 | 2.19 | 0.07 |
| | 9.00 | 664 | 690 | 26.16 | 2.05 | 2.13 | 0.08 |
| TNT | average | | | | 2.24 | 2.29 | 0.05 |
| TNT | reference data | | | | 2.37 km/s [2, 12] | | |
| HMX | 0.98 | 2451.7 | 2709 | 257.3 | 2.98 | 3.29 | 0.31 |
| | 2.13 | 1753 | 1759 | 6.3 | 2.84 | 2.85 | 0.01 |
| | 3.01 | 1490 | 1487 | 2.2 | 2.79 | 2.79 | 0.00 |
| | 4.98 | 1160 | 1167 | 6.8 | 2.71 | 2.73 | 0.02 |
| | 6.99 | 958 | 959 | 0.84 | 2.62 | 2.62 | 0.00 |
| | 9.00 | 827 | 855 | 28.06 | 2.55 | 2.64 | 0.09 |
| HMX | average | | | | 2.75 | 2.82 | 0.07 |
| HMX | reference data | | | | 2.97 km/s [12, 15] | | |

As already stated in Section 5.2.1, the convergent front does not cause much higher velocities than the planar front, as one might have expected. However, the convergent front induces slightly higher final velocities. The remarkable fact of Figure 5.9 is the increasing Gurney constant by concurrent decrease of the cylinder mass. The larger the mass of the cylinder, the lower the final wall velocities and respectively the Gurney constants. The same is true for TNT and HMX, regarding the values in Table 5.4. There is no value of M/C $= 1$ for the convergent front because the cylinder wall fractured in this simulation.

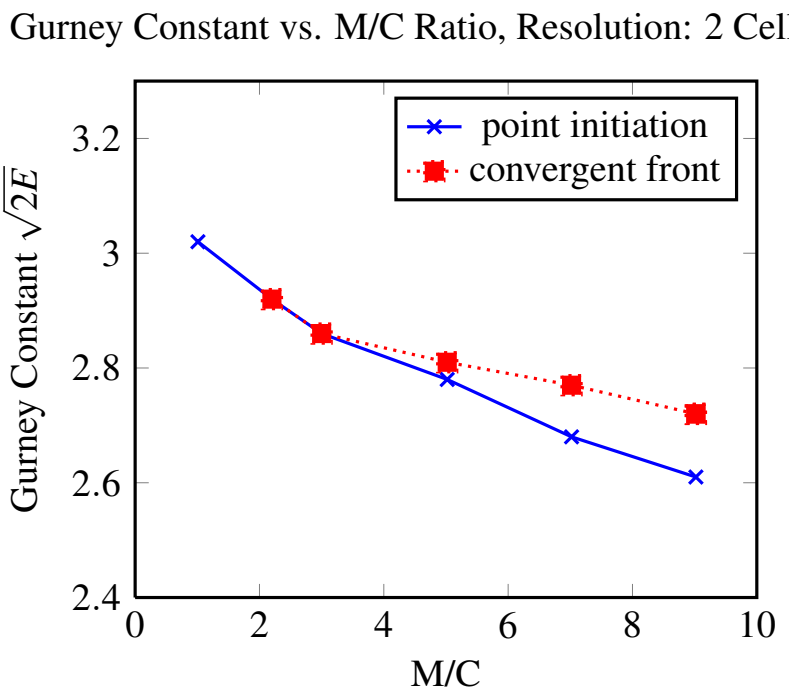


Figure 5.9: Comparison of point initiation and convergent front concerning Gurney constant over M/C ratios for a 5 cm charge of LX-14

**Effect of Size**

In order to check the results gathered from the 5 cm charge concerning the dependence of the Gurney constant on the M/C ratio, a similar simulation series was done with LX-14 15 cm charges over a range from $0.1 < \text{M/C} < 10$. Realizing an M/C ratio of 0.13, the cylinder wall had to be just one millimeter thin. That automatically leads to an early fracture of the cylinder during the expansion process. The 4 mm thick cylinder wall, required for an M/C ratio of 0.5, withstands the pressure almost without fracturing, regarding the convergent front. The cylinder wall of the same simulation for the point initiation fractured, so that value had not been considered any further. The same extends to the M/C ratio of 1.0 for the 5 cm charge. In general it can be stated that values were only considered, when the cylinder wall did not fracture during simulation. The results of both charge diameters are compared in Table 5.5.

The difference is again the absolute value. A general observation is that the Gurney constants of the 5 cm charge are always higher than the corresponding values for the 15 cm charge. Comparing values of M/C ratios, which were run with both charge diameters, the offset between the charge diameters is approximately between 0.2 and 0.5 km/s.

Table 5.5: Comparison of the results for the 5 cm charge and the 15 cm charge of LX-14

| Charge Diameter | M/C ratio | Final Velocity [m/s] | | | Gurney Constant [km/s] | | |
|---|---|---|---|---|---|---|---|
| | | point | convergent | difference | point | convergent | difference |
| 15 cm | 0.53 | 2327 | 2861 | 534 | 2.36 | 2.91 | 0.54 |
| | 0.99 | 2305 | 2363 | 58 | 2.82 | 2.89 | 0.07 |
| | 5.04 | 1087 | 1055 | 32 | 2.56 | 2.48 | 0.08 |
| | 9.98 | 728 | 738 | 10 | 2.36 | 2.39 | 0.03 |
| 5 cm | 1.00 | 2462 | 2776 | 314 | 3.02 | 3.41 | 0.93 |
| | 2.20 | 1778 | 1778 | 0.0 | 2.92 | 2.92 | 0.00 |
| | 3.00 | 1530 | 1528 | 2 | 2.86 | 2.86 | 0.00 |
| | 5.02 | 1183 | 1198 | 15 | 2.78 | 2.81 | 0.03 |
| | 7.02 | 978 | 1010 | 32 | 2.68 | 2.77 | 0.09 |
| | 9.02 | 846 | 883 | 37 | 2.61 | 2.72 | 0.11 |

However, considering the uncertainties of up to 70 m/s for the final velocity and therefore up to 0.1 km/s uncertainty for the Gurney constant, the offset could also be higher. Figure 5.10 illustrates the Gurney vs. M/C ratio correlation for the 15 cm cylinder.

Figure 5.10 shows the same trend as Figure 5.9. However, the values are different, and the convergent front does not always cause the higher velocities. As already mentioned, the values for the M/C ratio of 0.5 are noticeable, which refers most likely to the slight fragmentation of the cylinder wall during expansion. In addition, the final cylinder velocity for a point initiated M/C ratio of 0.53 did not differ significantly from the velocity for the simulation of M/C $= 0.99$. It turned out that the cylinder wall of the M/C $= 0.99$ simulation fractured only a little at the beginning of the cylinder. At first, that fact was found to be negligable, but the analysis showed a suspciously high velocities. Therefore, that value was discarded and is not shown in Figure 5.10.

### 5.2.3 Discussion of the Results of the Cylex Test Simulations

Concerning the simulations of the cylinder expansion test, no general advantage of a convergent front compared to a planar front can be deduced from these results. The calculated final wall velocities of the cylinder are mostly higher for the convergent front, but the Gurney constants are all in the same range of statistical uncertainties. However, there is a distinct trend regarding Gurney constants vs. M/C ratios. The higher the M/C ratio is, the lower are the final wall velocities and therefore the Gurney constants. The Gurney constants calculated for LX-14 are higher than for HMX. As HMX detonates faster and releases more energy, the Gurney constant should be higher than for LX-14, which consists only of 95.5 % HMX.

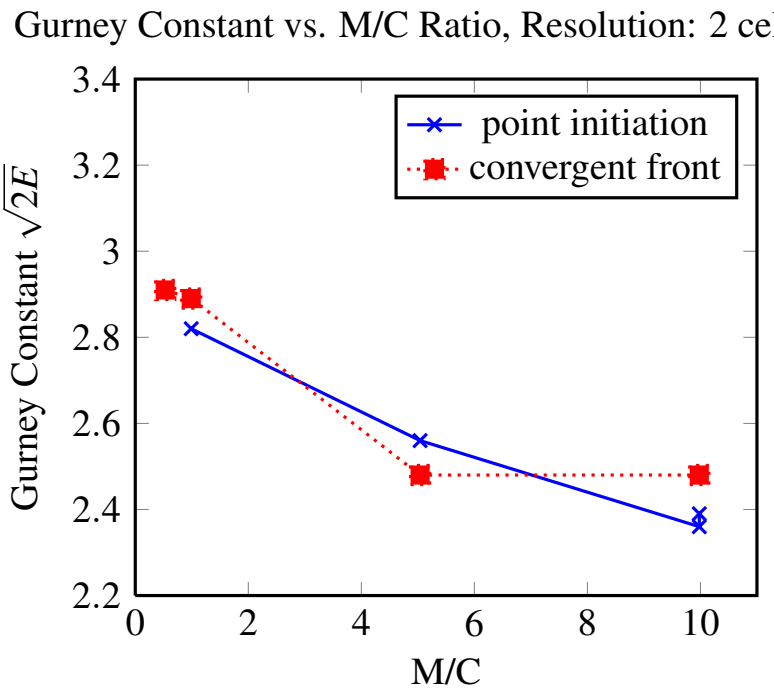


Figure 5.10: Results of the 15 cm charge of LX-14: Gurney vs. M/C ratio

This difference is illustrated by the reference data for these explosives in Table 5.4. The average of the calculated values for LX-14 is slightly higher than the reference data, whereas the average of the Gurney constant for HMX lies significantly below the reference value. As one would expect more divergent results comparing the different detonation fronts, the implementation of a convergent front by the use of an array of circumferential initiation points might not be a solution that represents actual situations. However, the calculated Gurney constants are in the range of the constants calculated with the estimates in Table 2.4, although there are possible uncertainties.

## 5.3 Validation of Andrews' Experiment

Subject of this section is the Andrews experiment. The effect of variation of the sleeve thickness is investigated for both configurations, the one with PBXN-110 and PBXN-111 and for the cylinder filled with TNT and LX-14. Afterwards, the effect of convergence on metal acceleration is analyzed and finally the total energy of the composite explosive is considered.

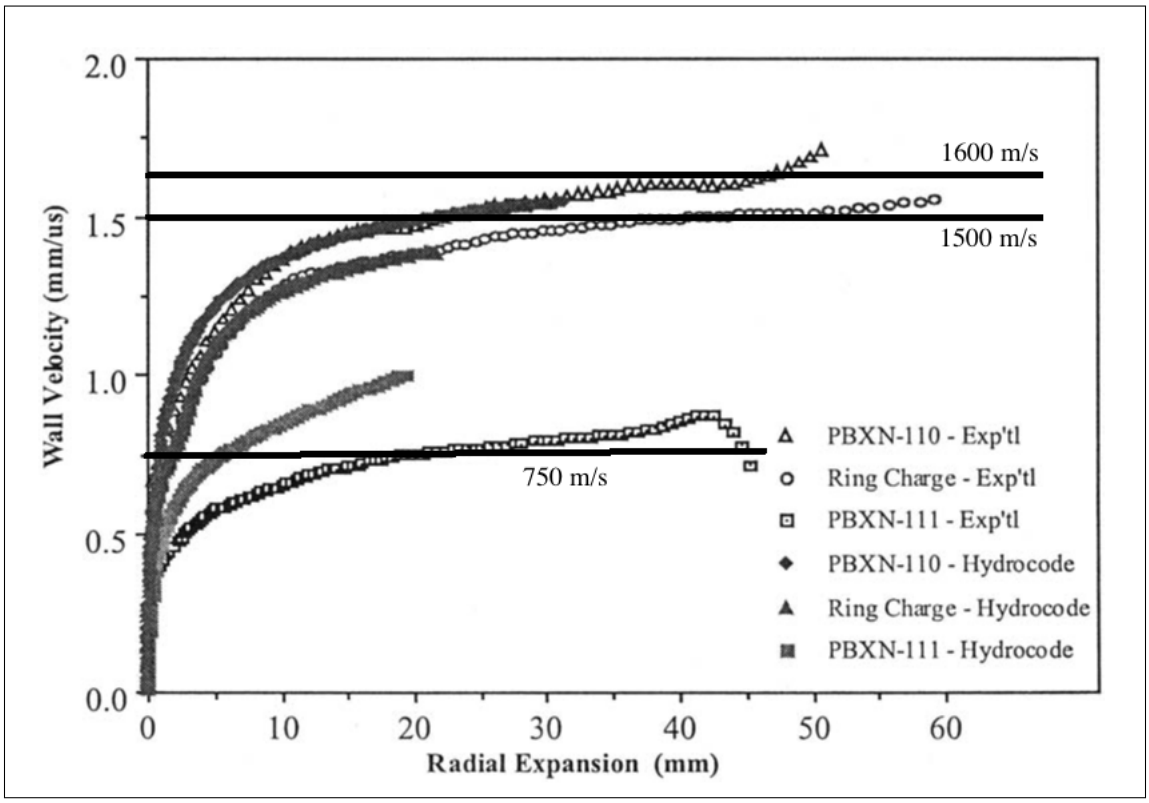


Figure 5.11: Reported velocities by Andrews (from [1])

First of all, the data gathered by Andrews is compared to the results of this work. His measured velocities are compared to the velocities measured in AUTODYN and are listed in Table 5.6. It must be noted that the velocities from Andrews experiment were read from the reported Figure 5.11.

Regardless of the minor differences, the values are in the same range and do not contrast strongly with each other. Therefore, the results of Andrews' experiment can be validated. Andrews determined according results of hydrocode calculations and experimental data for the ring charge and for the experiment with just PBXN-110. However, he detected a variance in results regarding the PBXN-111 charge. The experimental data is approximately 750 m/s, as

listed in Table 5.6, whereas a higher velocity, but still $v_{final} < 1000$ m/s, was calculated by the hydrocode. During this research, a final wall velocity of 934 m/s was calculated, which correlates to the result of Andrews' hydrocode calculation.

Table 5.6: Validation of the Andrews experiment with PBXN-111 and PBXN-110

| Charge | Final Wall Velocity [m/s] | |
|---|---|---|
| | Andrews' experiment | Simulations of this work |
| Ring charge | $\approx 1500$ | 1408 |
| only PBXN-111 | $\approx 750$ | 934 |
| only PBXN-110 | $\approx 1600$ | 1503 |

### 5.3.1 Variation of Sleeve Thickness

Andrews applied a 12.9 mm thick sleeve of PBXN-110 around the core of PBXN-111 in his original experiment and documented higher wall velocities in comparison to a cylinder just filled with PBXN-111. The results of reducing the sleeve thickness are presented in this section and illustrated in Figure 5.12.

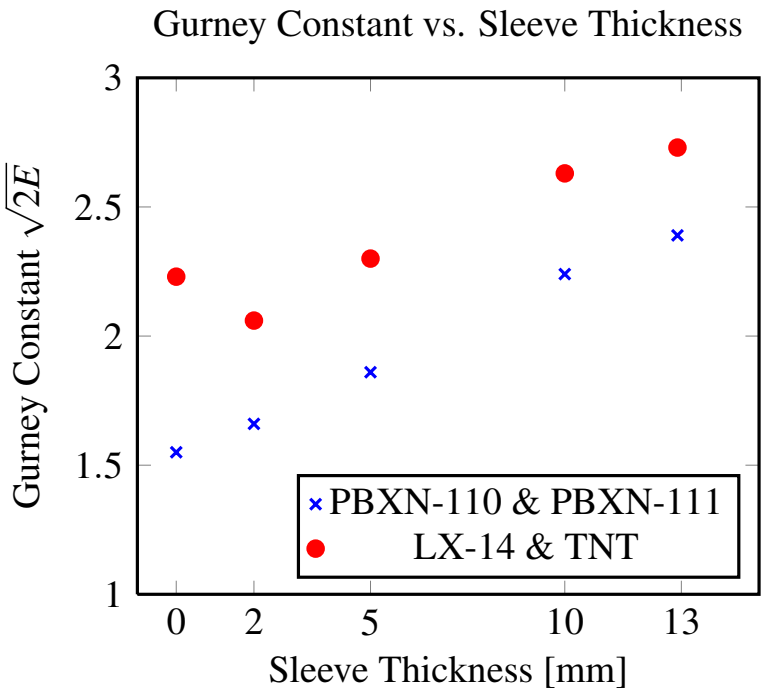


Figure 5.12: Effect of reducing the sleeve thickness on the Gurney constant

The thicker the sleeve of PBXN-110, the higher wall velocities are reached and the higher is the Gurney constant. The value for a sleeve thickness of 0 mm refers to the cylinder just filled with PBXN-111, respectively a pure charge of TNT. However, with such a thin sleeve as of 2 mm thickness, the Gurney constant can be increased from 1.55 km/s (no sleeve) to 1.66 km/s for the configuration of PBXN-111 with PBXN-110. Regarding the charge of TNT and LX-14, the Gurney constant also increases by sleeve thickness. The value for the TNT charge without any sleeve is salient, because it is higher than that for the configuration with a 2 mm sleeve of LX-14. Although the configuration with the sleeve provides more explosive energy, the charge of pure TNT seems to cause higher wall velocities. The reason for that could not be detected and is most likely an error caused by the problem setup. It is to believe that the Gurney constant for a cylinder filled with pure TNT is lower than for the configuration with a 2 mm sleeve of LX-14. Comparing the measured detonation velocities in the core and the sleeve, it is remarkable that these velocities do not differ wildly from each other, as shown in Figure 5.13.

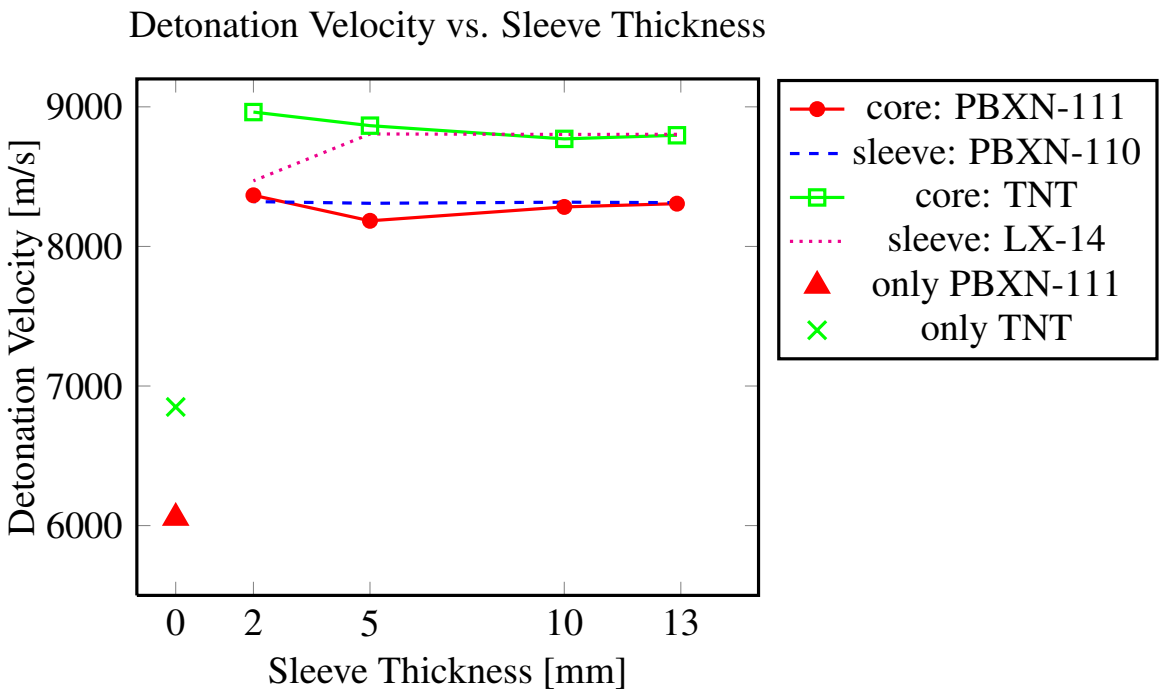


Figure 5.13: Effect of the sleeve thickness on detonation velocity

Especially the detonation velocity of the sleeve seems to be independent of its thickness. Comparing the velocities at the center line of the cylinder for the PBXN-111 core with a 12.9 mm sleeve to that with a 2 mm sleeve, the difference is only 60 m/s. The only value that contra-

dicts is the detonation value of the 2 mm thick TNT sleeve. The reason for that could not be detected. In addition, the detonation velocities for the cylinder filled with only on explosive were measured also along the center line and directly at the cylinder wall. The values for TNT correspond to the values of Table 2 in the Appendix. Though, the measured detonation velocity of PBXN-111, which is approximately 6.050 km/s, is slightly higher than the 5.775 km/s listed in Table 3. This increase is probably caused by the previous detonation of the Pentolite booster, which has a detonation velocity of 7.53 km/s, according to Table 3. Comparing the values for pure explosives with the values of the coaxial charge, the substantial increase in detonation velocity caused by a sleeve of higher detonation explosive is illustrated in Figure 5.13. Even by means of a thin sleeve, the detonation velocity along the center axis can be increased almost up to the detonation velocity of the sleeve.

### 5.3.2 Effect of Convergence on Plate Acceleration

A steel disk with an increased yield stress was put at the end of the cylinder for each configuration in order to measure its velocity and deduce an effect of convergence on metal acceleration. Due to inevitable deformation, even with an increased yield stress, the velocity was measured along the cylinder axis and at the upper edge of the disk. Deformation causes a difference in these velocities. Table 5.7 contains the measured disk velocities depending on the sleeve thickness for both the configuration with the explosives used by Andrews and the modified configuration regarding the investigated explosives. The thicker the sleeve, the higher are the velocities of the disk due to the increasing total energy of the composite.

In addition, there is a column containing the ideal disk velocity in Table 5.7. This refers to the velocity calculated by the Gurney equation for the open face sandwich configuration, Equation 2.10, with the Gurney constant calculated by means of the simulations of this chapter. However, not the whole charge has an effect on the acceleration on the plate at the end, so the M/C ratio has to be modified. M is now the mass of the disk and C has to be recalculated. Only a part of the explosive affects the metal acceleration. That part is the so called effective charge. The mass of the effective charge $C_{eff}$ can be calculated with the use of Benham's Equation 2.11 in Section 2.4. The ideal, theoretically possible velocity of the steel disk is then obtained by plugging in M/$C_{eff}$ in Equation 2.10. The results are illustrated in Figure 5.16. The velocities that were measured along the cylinder axis by fixed gauges are marked as "center" and the velocities that were measured at the upper edge of the disk are marked as "edge". These results already elucidate the problem of deformation.

Table 5.7: Effect of convergence on metal acceleration

| Configuration | Sleeve thickness [mm] | Final velocity of the disk [m/s] center line | upper edge | ideal* |
|---|---|---|---|---|
| PBXN-110 & PBXN-111 | 12.9 | 560.46 | 586.58 | 771.40 |
| | 10 | 507 | 536 | 723 |
| | 5 | 436 | 437 | 598 |
| | 2 | 368 | 392 | 532 |
| | 0 | 378 | 384 | 496 |
| LX-14 & TNT | 12.9 | 528.06 | 550.88 | 826.35 |
| | 10 | 494 | 511 | 798 |
| | 5 | 396 | 425 | 701 |
| | 2 | 351 | 385 | 634 |
| | 0 | 443 | 455 | 693 |

*based on Gurney equation and estimated $\sqrt{2E}$

Although the yield stress of the steel disk was increased, it still deforms. An ideal plate would move uniformly along the cylinder axis, even when driven by a convergent front that does not impinge upon all over the disk's surface at once. The difference of the velocities measured at the center line and at the upper edge illustrate the uneven movement of the disk caused by deformation.

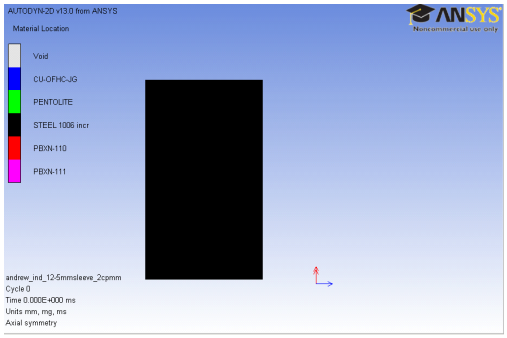


Figure 5.14: Initial shape of the steel disk

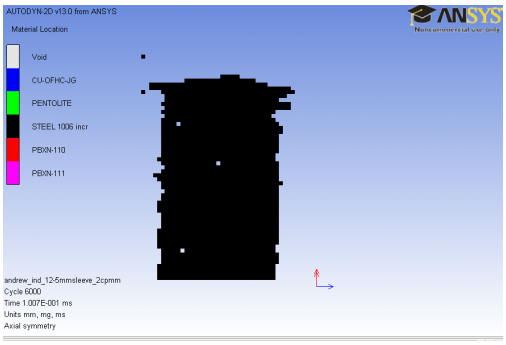


Figure 5.15: Shape of the steel disk after being accelerated

Theoretically, much higher velocities are possible, as is shown by the straight lines, marked as ideal velocities. Obviously, deformation and gas leakage are not yet considered by these ideal approximations. The shape of the disk before at the beginning of the simulation is shown in

Figure 5.14, whereas the deformation of the disk after being accelerated is shown in Figure 5.15. The figures were taken from a simulation of the original Andrews configuration with a core of PBXN-111 surrounded by a 12.9 mm sleeve of PBXN-110. In order to concentrate on the steel disk, every other material has been hidden. In addition, these figures only display the part of the disk from the center line of the cylinder to the upper edge. The time stamps of these figures clarify the initial and final state of the disk. Due to the earlier collision of the sleeve featuring the higher detonation velocity with the disk, especially the upper edge deforms even with the modified yield stress.

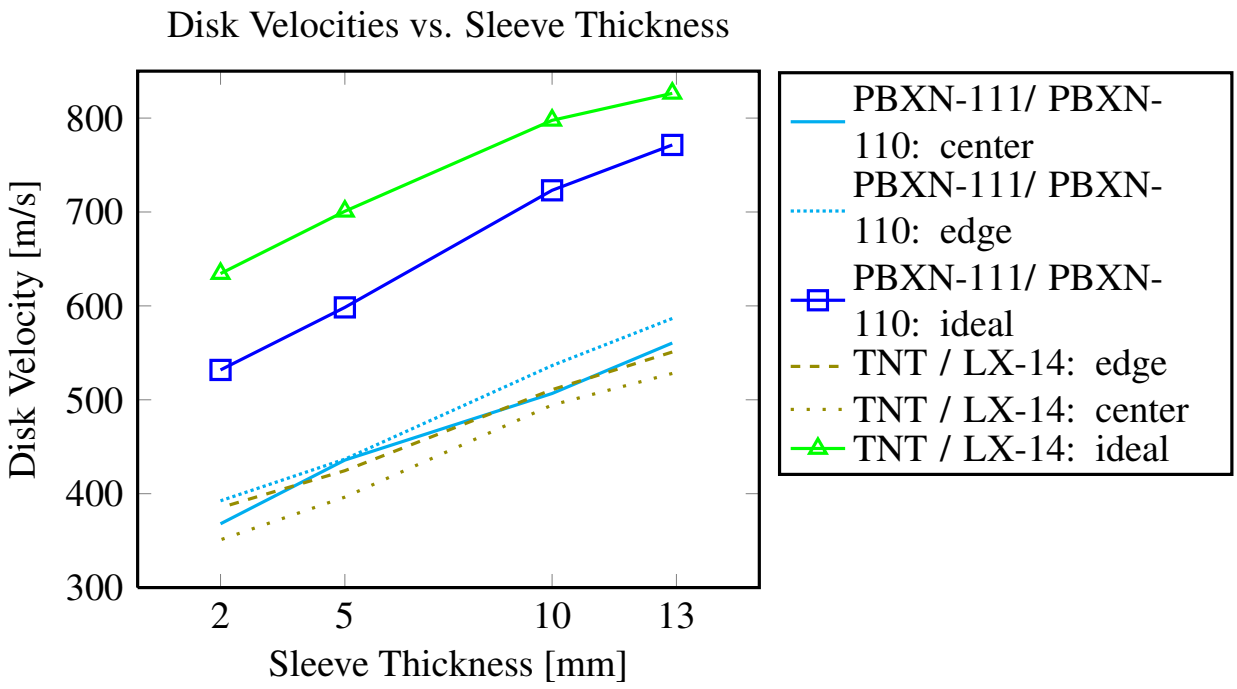


Figure 5.16: Ideal and measured disk velocities vs. sleeve thickness

### 5.3.3 Energy Averaging

In order to compare the outcome of the different configurations concerning the Andrews experiment, the total energy provided by the composite charge has to be considered. The plot for the energy vs. sleeve thickness is shown in Figure 5.17. As one would expect, the configurations with thicker sleeves provide more total energy due to the substantial mass of the higher detonation explosive. However, these results show the possibility of increasing the total energy of the charge by 0.3 MJ, respectively 0.4 MJ for the TNT/LX-14 configuration, by replacing the outer 2 mm of the charge with a faster detonating explosive.

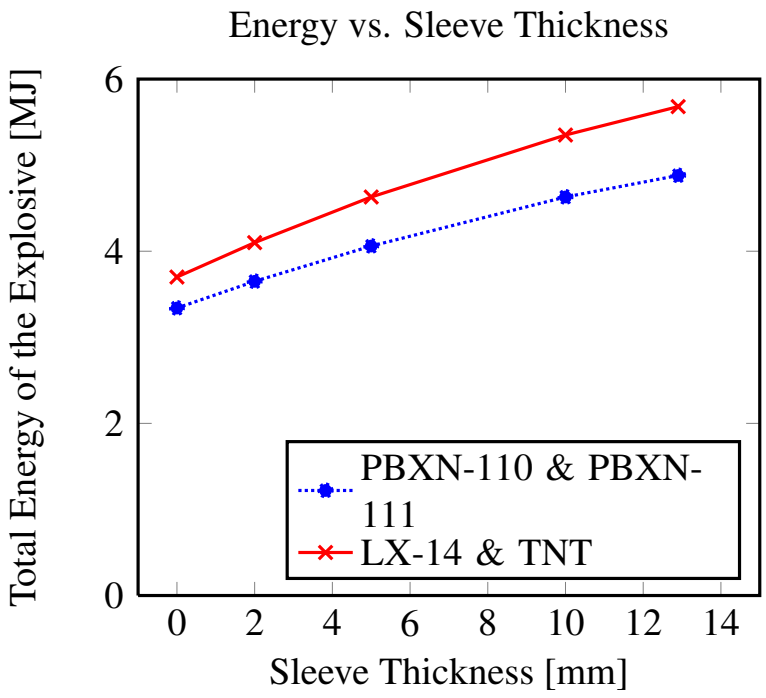


Figure 5.17: Total energy provided by the charge depending on the ratio of explosives.

The Gurney constant was found to be a function of the total explosive energy of the composite charge. This relation is shown in Figure 5.18. Both explosive composites TNT / LX-14 and PBXN-111 / PBXN-110 have been considered. The higher the amount of provided energy the higher are the Gurney constants of the composite charge.

The ratios of energy E derived from $\sqrt{2E}$ over the total energy of the explosive for the coaxial charges are listed in Table 9 and Table 10 of the Appendix. Depending on sleeve thickness, the ratio is between 0.41 (2 mm sleeve) and 0.61 (12.9 mm sleeve) for the configuration of PBXN-111 with PBXN-110 and between 0.53 (2 mm sleeve) and 0.72 (12.9 mm sleeve) for the configuration of TNT with LX-14. As a consequence, the proportion of charge that causes cylinder expansion differs from approximately 40% to 70%.

**Investigation of the Outcome of the Andrews Experiment**

In order to compare the different outcomes of cylinders one just filled with PBXN-111 and one with a surrounding sleeve of PBXN-110 the setup for the Andrews experiment had been slightly modified. A magnesium block had been set directly at the end of the cylinder with no gap between the block and the explosive.

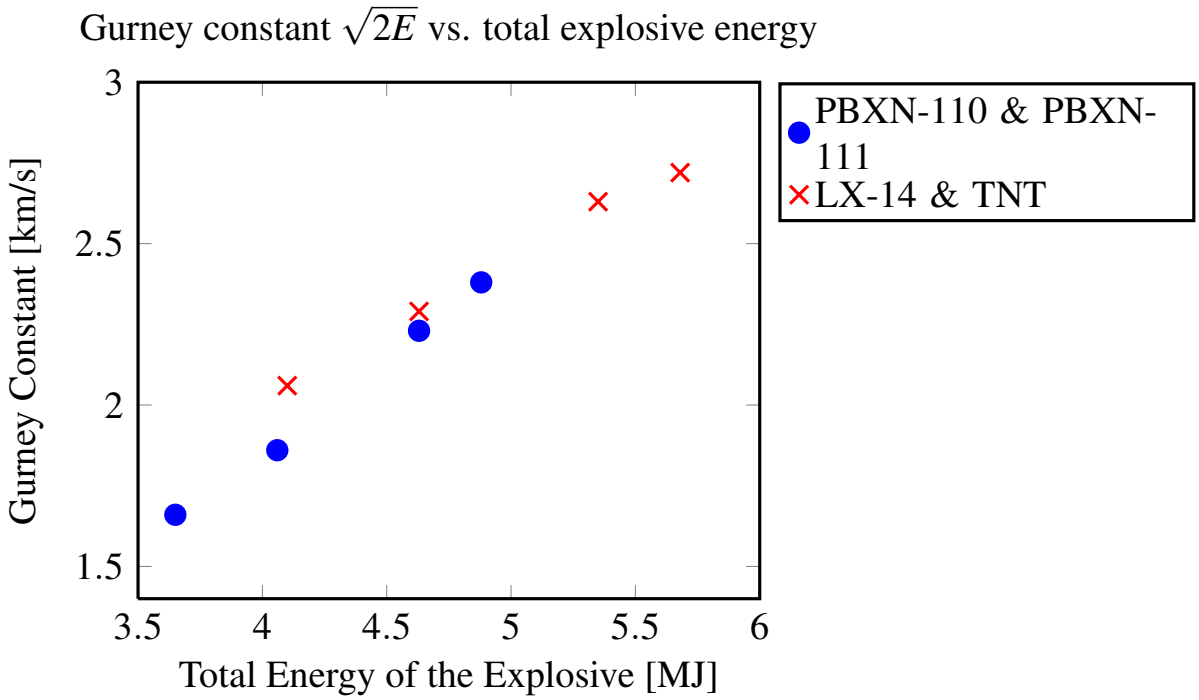


Figure 5.18: Gurney constant as a function of the total energy provided by the explosive composite.

The cylinder walls had been thickened up in order to focus the explosive energy. Magnesium does not deform in a way a block of heavy metal would do. The explosive rather burn a cavity in the material. The results of the charge referring to the original Andrews experiment are presented in Figure 5.19. The cavity caused by a charge of pure PBXN-111 is shown in Figure 5.20. These snapshots were almost taken at the same time as can easily be determined by looking at the time step of these figures. The two displayed gauges for each figure illustrate the cavity's extent. Fixed gauges were used to measure the height and depth of that cavity. In Figure 5.19 the gauges 74 and 183 are displayed.

An X-array of fixed gauges was arranged along the center line, beginning with gauge one at the intersection of the explosive with the magnesium block. From that, another gauge was put every single millimeter, which leads to depth of 73 mm. At the end of the simulation, a Y-array of gauges was arranged at the X-coordinate of the maximum height of the cavity. Gauge 113 is the first of that array. Therefore, the cavity of Figure 5.19 ist 69 mm high. Applying the same method of measurement to Figure 5.20, the extent of that cavity can be obtained as only 35 mm deep and 47 mm high.

It has to be stated that these results may not be as meaningful as expected. The arranged model in AUTODYN turned out to be too small to let the magnesium block expand in an unimpeded manner. Therefore, the target expansion is restrained by the boundary condition. This could affect the results. In summary, the issue of the outcome of the Andrews experiment could not be investigated conclusively. Hence, the presented extent of the cavities should be reviewed and not be taken as final.

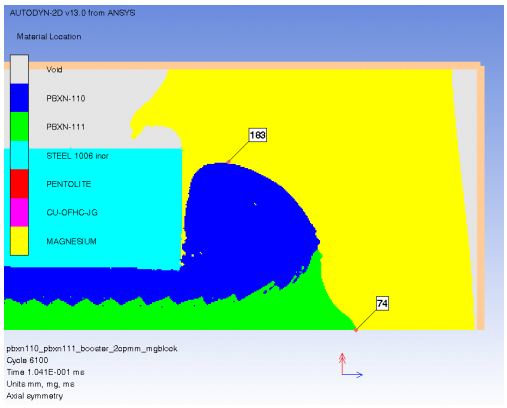


Figure 5.19: Outcome of the original Andrews configuration

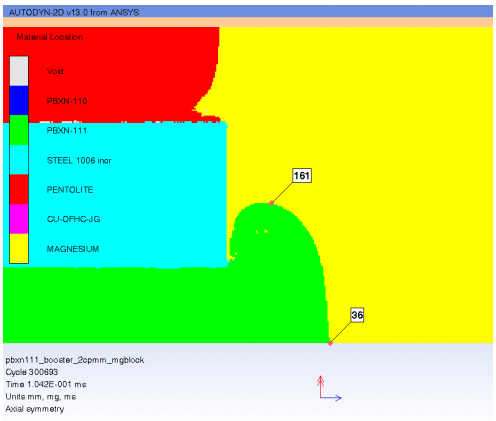


Figure 5.20: Outcome of a cylinder filled with PBXN-111

### 5.3.4 Discussion of the Results of the Andrews Experiment

First of all, the data gathered by Andrews in a real experiment could be validated with hydrocode simulations. Although the values do not correspond exactly, the general trend of the values could be approved for the coaxial charge and the charges of pure explosive.

The investigation of sleeve thickness resulted in effects on Gurney constants even of thin sleeves. The Gurney constant could be increased from 1.55 km/s (pure PBXN-111) to 2.28 km/s by means of a 2 mm sleeve of PBXN-110. In general it can be stated that the thicker the sleeve is, the higher are the calculated Gurney constants for the configuration. However, the detonation velocity was found to be almost independent from sleeve thickness. The measured velocities in the sleeves were nearly constant, despite variations in thickness. Even the velocities measured in the core along the center line were found to be nearly constant. In fact, 8306 m/s were measured in the core of PBXN-111 for the configuration surrounded by a 12.9 mm sleeve of PBXN-110 and 8366 m/s were measured with a sleeve thickness of only 2 mm. Regarding the varying composition of the charge, the total energy provided by the explosive system increased

with the sleeve thickness. That is reasonable due to the increasing amount of the faster detonating explosive, which provides more explosive energy. The thicker the sleeve, the higher the amount of provided total energy and therefore the higher the Gurney constants.

Although the problem of fragmentation of the steel disk reported by Andrews could be overcome, the deformation and the loss of energy due to gas leakage prevent the disk from achieving the theoretically possible velocity. However, the thicker the sleeve is, the higher are the velocities the disk can reach. The effective outcome of the coaxial charge could even not be investigated with the configuration with the magnesium block due to difficulties with the implementation of the problem in AUTODYN. As a preliminary result it can be stated that the outcome of the coaxial charge differs from the outcome of a charge of a pure explosive. However, the exact values documented in this section can not be taken as absolute values.

All reported results correspond to the composite of PBXN-111 with PBXN-110 and to the configuration with LX-14 and TNT. No difference in the trend of results could be detected concerning different explosives.

# CHAPTER 6:
# Conclusions

This work makes a contribution to the research field of metal acceleration by the means of detonations and investigates the effect of convergence. Although Gurney published his model in the early 1940s, there is still an interest in the validation of the model and the possible applications. Concerning Gurney, there was only the report by Koch and co-worker [12] during the last decade.

The objective of this study was directed toward determining whether there is a significant difference in results comparing convergent and planar detonation fronts and the effects on metal acceleration quantified by the value of the Gurney constant $\sqrt{2E}$. In order to allow universality of results, different explosives and resolutions were examined for a 5 cm charge and a 15 cm charge.

Andrews and co-worker [1] set up a coaxial charge and documented measured velocities of the metal. Computational techniques developed for this study are found to accurately predict experimental cylinder expansion results reported by Andrews for PBXN-110, PBXN-111 and a coaxial charge of PBXN-110 with PBXN-111. In addition, the variation of sleeve thickness was investigated, because Andrews used a relatively thick sleeve. The thicker the sleeve, the higher the Gurney constant, whereby even a thin sleeve of 2 mm was found to be more effective for achieving higher velocities than a charge of a pure explosive. The convergent detonation front velocity appears to be invariant with outer sleeve thickness. The velocities measured in the core and the sleeve stayed nearly constant throughout the series of sleeve thickness reduction. Convergent detonation fronts realized by coaxial charges were found to affect the Gurney constant as expected. Furthermore, the results of a coaxial charge of LX-14 and TNT were found to agree with those already validated for PBXN-110 and PBXN-111.

The effect of sweeping circumferential initiation on metal acceleration affected by "programmed" detonation points is found not to differ significantly from point and planar initiation. The calculated values for $\sqrt{2E}$ comparing convergent and divergent detonation fronts could not illustrate the ability of convergent fronts to accelerate metal faster. In these cases the mach stem that forms affects a minute fraction of the total detonation front. This way of implementing a convergent front is found to be insufficient for each examined explosive.

Gurney constants for LX-14, TNT and HMX are found to agree with those listed in Table 2.5 and estimated by empirical relationship proposed by Cooper, Koch and others. Though, even the reported values differ. In fact, the Gurney constant for HMX was found to be lower than for LX-14. As HMX contains more energy and detonates faster, it should show a better ability to accelerate metal. The reference values confirm the assumption, however, the simulations arrived at a different result. It has to be stated that the calculated Gurney constants of this work differ depending on the investigated configuration. However, they are all in the same range and correspond to already published values. In addition, the Gurney constant was found to be a function of the M/C ratio, at least for the examined cylindrical configuration. The value for $\sqrt{2E}$ decreases as the ratio increases, which was not expected due to the fact that the Gurney constant should be a a specific value for a certain material. Furthermore, it appears to be a function of the total energy provided by the explosive charge.

The issue of metal acceleration concerning a steel disk at the end of a cylinder could not be investigated closely. The problem of fragmentation reported by Andrews was overcome, however, the deformation of the disk and the leakage of product gases due to the geometry of the cylinder need further consideration. It is assumed that by overcoming these problems, the theoretically possible velocity calculated from the Benham equation could be achieved.

However, the predicted effective charge length did not match the length determined in this work. Following Benham, the effective charge length for a cylindrical charge with no confinement would be half as long as detected in this work. The results have to be adjusted in order to identify the absolute effective length of charge.

# CHAPTER 7:
# Recommendations for Further Studies

Some issues of this work need to be considered more closely in further works and researches. In general, it can be stated that this work only presents data and information gathered from numerical simulations. These results have to be validated by experimental investigations. In order to improve the model setup of the simulation, experimental and calculated results have to be converged. In fact, numerical simulations should always be included in an iterative process of experiments and model improvements.

For one thing, it is important to detect possible errors of the model setup by comparing calculated with experimental results. For another thing, unexpected results such as the dependence of the Gurney constant on the M/C ratio, have to be investigated in experiments. As long as the programmed model setup has not been validated with any experimental results, there could be errors in the setup. However, the experimental results of Andrews' experiment could be validated.

Regarding AUTODYN simulations of this work, it often occurred a so-called "Euler cell over-emptied" error, which immediately terminates the simulation. Although it is possible to let the simulation proceed, the origin of this error should be detected and solutions have to be found in order to avoid this error. In addition, the effect of that error on the result could not be determined in this work.

The velocity measurement in AUTODYN has to be reconsidered. It is not clear, whether in this work the absolute final velocities were measured. Corresponding to Figure 4.4 and Figure 4.5 in Chapter 4, there is a difference in velocity depending on how many fixed gauges were taken into account. Besides, does only one column of fixed gauges arbitrarily arranged at the middle of the cylinder allow an estimation for the final velocity of the cylinder wall? One column of fixed gauges corresponds to one moving gauge in the cylinder wall. The difference in final velocities gathered from a number of arrays of fixed gauges along the cylinder should be investigated.

The problem of launching a steel disk by detonation has to be reconsidered. Even though it was managed to accelerate a disk without fracturing, the effects of material deformation and energy loss by gas leakage need to be further investigated. Additionally Benham's equation regarding the effective charge length for a configuration with a confinement is worth to be further analyzed

by conducting more simulations that investigate the lengths between 40 and 90 mm, assuming a charge of 5 cm in diameter.

The simulations for the investigation of the outcome of the Andrews experiment could not be finished for lack of time. The setup with the magnesium block has to be reconsidered and possibly improved in order to investigate the deformation of the magnesium. There has to be enough space between the magnesium block and the boundaries in order to allow expansion. In addition, Koch's analysis of energy distribution should be experimentally examined.

# APPENDIX - Calculation of $\Phi$

In this chapter the calculation of $\Phi$ is explained by taking the example of a representative of the CHNO explosives. The chemical formula of HMX is $C_4H_8O_8N_8$.
Kamlet and Jacobs [14] assume a predominant formation of carbon dioxide $CO_2$, rather than carbon monoxide CO, which leads to the chemical reaction

$$C_4H_8O_8N_8 \rightarrow 4N_2 + 4H_2O + 2CO_2 + 2C \tag{1}$$

In order to calculate $\Phi$, the first step is to determine Q in cal/g.
The heat of detonation represents the amount of energy which is released by the chemical reaction of the explosive undergoing detonation regardless of any other possible energy input.

$$\Delta H_d^0 = \sum \Delta H_f^0(detonationproducts) - \sum \Delta H_f^0(explosive)$$

$$\Delta H_d^0 = \left[4\Delta H_f^0(N_2) + 4\Delta H_f^0(H_2O) + 2\Delta H_f^0(CO_2) + 2\Delta H_f^0(C)\right] - \Delta H_f^0(HMX)$$

$$\Delta H_d^0 = [4(0) + 4(-68.3174) + 4(-94.0518) + 2(0) - (+17.93)]\ \tfrac{kcal}{g \cdot mole}$$ [7]

$$\Delta H_d^0 = \text{-}479.3032\ \tfrac{kcal}{g \cdot mole}$$

For further calculation the energy is required in $\frac{cal}{g}$. Therefore, the molecular weight (MW) of HMX has to be provided. This can easily be done with respect to Table 1 and by knowing the chemical formula of HMX.

$$MW_{HMX} = [4(C) + 8(H) + 8(O) + 8(N)]\ \tfrac{g}{mole}$$

$$MW_{HMX} = [4(12.01) + 8(1.008) + 8(14.00) + 8(16.0)]\ \tfrac{g}{mole}$$

$$MW_{HMX} = 296.2 \tfrac{g}{mole}$$

$$\Rightarrow Q = \tfrac{\Delta H_d^0}{296.2} \Rightarrow Q = -1618.17 \tfrac{cal}{g}$$

Calculating the number of moles of gaseous detonation products per gram explosive (N) is the next step. Using the right side of Equation 1 and just taking into account the gaseous products

[7] Heat of formation data taken from Table 9.2 on page 125 of Cooper [2]

Table 1: Molecular weights

| Atom / molecule | Molecular weight $\frac{g}{mole}$ |
|---|---|
| C | 12.01 |
| H | 1.008 |
| N | 14.00 |
| O | 16.00 |
| $N_2$ | 28.016 |
| $H_2O$ | 18.016 |
| $CO_2$ | 44.01 |

leads to:
$4N_2 + 4H_2O + 2CO_2 = 10$ moles gas per mole HMX

$N = \frac{10}{MW} = \frac{10}{296.2} = 0.03376$ moles gas per gram of explosive

Last step is calculating the molecular weight of gaseous detonation products (M):
Once again just the gaseous detonation products of Equation 1 are regarded. Using Table 1 results in:

$M = \frac{4(N_2)+4(H_2O)+2(CO_2)}{10}$

$M = \frac{4(28.016)+4(18.016)+2(44.01)}{10} = 27.2148 \frac{g}{mole}$

Putting the values of Q, N and M together further calculation of $\Phi$ is straightforward:
$\Phi = NM^{1/2}Q^{1/2} = 7.08$

# APPENDIX - Material Models

All materials used in the calculations of this work are listed in Table 2–4. Please note the units of the material properties. To avoid deformation the Steel 1006 from the AUTODYN library was modified. "Steel 1006 incr" has an increased yield stress of 3.5e+015 kPa.

Table 2: Explosives used in calculations (I)

| | **LX-14** | **TNT** | **HMX** | Unit |
|---|---|---|---|---|
| Reference Density | 1.835 | 1.630 | 1.891 | $g/cm^3$ |
| EOS | JWL | JWL | JWL | |
| Parameter A | 8.261e+008 | 3.7377e+008 | 7.7828e+008 | *kPa* |
| Parameter B | 1.724e+007 | 3.7471e+006 | 7.071401e+006 | *kPa* |
| Parameter R1 | 4.55 | 4.15 | 4.20 | *none* |
| Parameter R2 | 1.32 | 0.90 | 1.00 | *none* |
| Parameter W | 0.38 | 0.35 | 0.30 | *none* |
| C-J Detonation velocity | 8.80e+003 | 6.93e+003 | 9.110001e+003 | $m/s$ |
| C-J Energy / unit volume | 1.02e+007 | 6.00e+006 | 1.05e+007 | kJ/$m^3$ |
| C-J Pressure | 3.70e+007 | 2.10e+007 | 4.20e+007 | *kPa* |
| Burn on compression fraction | 0.00 | 0.00 | 0.00 | *none* |
| Pre-burn bulk modulus | 0.00 | 0.00 | 0.00 | *kPa* |
| Adiabatic constant | 0.00 | 0.00 | 0.00 | *none* |
| Auto-convert to Ideal Gas | Yes | Yes | Yes | |
| Additional Options (Beta) | None | None | None | |
| Strength | None | None | None | |
| Failure | None | None | None | |
| Erosion | None | None | None | |
| Cutoffs | | | | |
| Maximum Expansion | 0.10 | 0.10 | 0.10 | *none* |
| Minimum Density Factor | 1.00e–006 | 1.00e–006 | 1.00e–006 | *none* |
| Minimum Density Factor (SPH) | 0.20 | 0.20 | 0.20 | *none* |
| Maximum Density Factor (SPH) | 3.00 | 3.00 | 3.00 | *none* |
| Minimum Soundspeed | 1.00e–006 | 1.00e–006 | 1.00e–006 | $m/s$ |
| Maximum Soundspeed (SPH) | 1.01e+020 | 1.01e+020 | 1.01e+020 | $m/s$ |
| Maximum Temperature | 1.01e+020 | 1.01e+020 | 1.01e+020 | $K$ |

Table 3: Explosives used in calculations (II)

| | **PBXN-110** | **PBXN-111** | **Pentolite** | Unit |
|---|---|---|---|---|
| Reference Density | 1.672 | 1.780 | 1.700 | $g/cm^3$ |
| EOS | JWL | JWL | JWL | |
| Parameter A | 9.504e+008 | 6.4493e+008 | 5.4094e+008 | *kP*a |
| Parameter B | 1.098e+007 | 3.9774e+005 | 9.372601e+006 | *kPa* |
| Parameter R1 | 5.00 | 5.40 | 4.50 | *none* |
| Parameter R2 | 1.40 | 1.00 | 1.10 | *none* |
| Parameter W | 0.30 | 0.20 | 0.35 | *none* |
| C-J Detonation velocity | 8.311e+003 | 5.775e+003 | 7.530e+003 | $m/s$ |
| C-J Energy / unit volume | 8.70e+006 | 5.40e+006 | 8.100001e+006 | kJ/$m^3$ |
| C-J Pressure | 2.75e+007 | 1.30e+007 | 2.55e+007 | *kPa* |
| Burn on compression fraction | 0.00 | 0.00 | 0.00 | *none* |
| Pre-burn bulk modulus | 0.00 | 0.00 | 0.00 | *kPa* |
| Adiabatic constant | 0.00 | 0.00 | 0.00 | *none* |
| Auto-convert to Ideal Gas | Yes | Yes | Yes | |
| Additional Options (Beta) | None | None | None | |
| Strength | None | None | None | |
| Failure | None | None | None | |
| Erosion | None | None | None | |
| Cutoffs | | | | |
| Maximum Expansion | 0.10 | 0.10 | 0.10 | *none* |
| Minimum Density Factor | 1.00e–004 | 1.00e–004 | 1.00e–006 | *none* |
| Minimum Density Factor (SPH) | 0.20 | 0.20 | 0.20 | *none* |
| Maximum Density Factor (SPH) | 3.00 | 3.00 | 3.00 | *none* |
| Minimum Soundspeed | 1.00e–006 | 1.00e–006 | 1.00e–006 | $m/s$ |
| Maximum Soundspeed (SPH) | 1.01e+020 | 1.01e+020 | 1.01e+020 | $m/s$ |
| Maximum Temperature | 1.01e+020 | 1.01e+020 | 1.01e+020 | *K* |

Table 4: Data of inert materials used in this work

| | **CU-OFHC-JC** | **Steel 1006 incr** | Unit |
|---|---|---|---|
| Reference Density | 8.93 | 7.896 | $g/cm^3$ |
| EOS | Shock | Shock | |
| Gruneisen coefficient | 2.02 | 2.17 | *none* |
| Parameter C1 | 3.94e+003 | 4.569e+003 | $m/s$ |
| Parameter S1 | 1.489 | 1.490 | *none* |
| Parameter Quadratic S2 | 0.00 | 0.00 | $s/m$ |
| Relative volume, VE/V0 | 0.00 | 0.00 | *none* |
| Relative volume, VB/V0 | 0.00 | 0.00 | *none* |
| Parameter C2 | 0.00 | 0.00 | $m/s$ |
| Parameter S2 | 0.00 | 0.00 | *none* |
| Reference Temperature | 300.00 | 300.00 | $K$ |
| Specific Heat | 382.999969 | 451.999969 | $J/kgK$ |
| Thermal Conductivity | 0.00 | 0.00 | $J/mKs$ |
| Strength | Johnson Cook | Johnson Cook | |
| Shear Modulus | 4.60e+007 | 8.180001+007 | $kPa$ |
| Yield Stress | 9.00e+004 | 3.50e+015 | $kPa$ |
| Hardening Constant | 2.92e+005 | 2.75e+005 | $kPa$ |
| Hardening Exponent | 0.31 | 0.36 | *none* |
| Strain Rate Constant | 0.025 | 0.022 | *none* |
| Thermal Softening Exponent | 1.09 | 1.00 | *none* |
| Melting Temperature | 1.356e+003 | 1.811e+003 | $K$ |
| Res. Strain Rate (/s) | 1.00 | 1.00 | *none* |
| Strain Rate Correction | 1st Order | 1st Order | |
| Failure | None | None | |
| Erosion | None | None | |
| Cutoffs | | | |
| Maximum Expansion | 0.10 | 0.10 | *none* |
| Minimum Density Factor | 1.00e–004 | 1.00e–004 | *none* |
| Minimum Density Factor (SPH) | 0.20 | 0.20 | *none* |
| Maximum Denity Factor (SPH) | 3.00 | 3.00 | *none* |
| Minimum Soundspeed | 1.00e–006 | 1.00e–06 | $m/s$ |
| Maximum Soundspeed (SPH) | 1.01e+020 | 1.01e+020 | $m/s$ |
| Maximum Temperature | 1.01e+020 | 1.01e+020 | $K$ |

THIS PAGE INTENTIONALLY LEFT BLANK

# APPENDIX - Simulation Data

The gathered data from all simulations is listed in the tables of this section. The data for the cylinder expansion test simulations (Table 5 and Table 6) is followed by the results of the simulations concerning the Andrews configuration (Table 7 to Table 11).

Table 5: Data of the cylex test simulations for a 5 cm charge

| explosive | M [g] | C [g] | M/C | wall velocity [m/s] point | wall velocity [m/s] convergent | Gurney constant [km/s] point | Gurney constant [km/s] convergent | $V/\sqrt{2E}$ point | $V/\sqrt{2E}$ convergent | regarded expansion [mm] point | regarded expansion [mm] convergent |
|---|---|---|---|---|---|---|---|---|---|---|---|
| LX-14 | 1140 | 1134 | 1.01 | 2462 | 2776 | 3.02 | 3.41 | 815.06 | 815.06 | 122 | 122 |
| | 2492 | 1134 | 2.20 | 1778 | 1778 | 2.92 | 2.92 | 608.86 | 608.86 | 126 | 122 |
| | 3407 | 1134 | 3.00 | 1530 | 1528 | 2.86 | 2.86 | 534.19 | 534.19 | 120 | 124 |
| | 5693 | 1134 | 5.02 | 1183 | 1198 | 2.78 | 2.81 | 425.62 | 425.62 | 128 | 132 |
| | 7966 | 1134 | 7.02 | 978 | 1010 | 2.68 | 2.77 | 364.55 | 364.55 | 114 | 124 |
| | 10227 | 1134 | 9.02 | 846 | 883 | 2.61 | 2.72 | 324.13 | 324.13 | 116 | 122 |
| TNT | 998 | 1008 | 0.99 | 1989 | 2133 | 2.43 | 2.60 | 819.21 | 819.21 | 118 | 110 |
| | 2492 | 1008 | 2.47 | 1343 | 1346 | 2.32 | 2.32 | 580.04 | 580.04 | 124 | 130 |
| | 3024 | 1008 | 3.00 | 1233 | 1223 | 2.31 | 2.29 | 534.52 | 534.52 | 128 | 132 |
| | 5021 | 1008 | 4.98 | 945 | 954 | 2.21 | 2.23 | 427.13 | 427.13 | 128 | 118 |
| | 031 | 1008 | 6.98 | 776 | 801 | 2.12 | 2.19 | 365.75 | 365.75 | 116 | 122 |
| | 9075 | 1008 | 9.00 | 664 | 690 | 2.05 | 2.13 | 324.39 | 324.39 | 104 | 120 |
| HMX | 1140 | 1169 | 0.98 | 2452 | 2709 | 2.98 | 3.29 | 823.33 | 823.33 | 104 | 112 |
| | 2492 | 1169 | 2.13 | 1753 | 1759 | 2.84 | 2.85 | 616.42 | 616.42 | 120 | 122 |
| | 3518 | 1169 | 3.01 | 1490 | 1487 | 2.79 | 2.79 | 533.81 | 533.81 | 120 | 126 |
| | 5817 | 1169 | 4.98 | 1160 | 1167 | 2.71 | 2.73 | 427.33 | 427.33 | 132 | 130 |
| | 170 | 1169 | 6.99 | 958 | 959 | 2.62 | 2.62 | 365.42 | 365.42 | 120 | 122 |
| | 10522 | 1169 | 9.00 | 827 | 855 | 2.55 | 2.64 | 324.43 | 324.43 | 122 | 116 |

Table 6: Data of the cylex test simulations for a 15 cm charge of LX-14

| M [g] | C [g] | M/C | wall velocity [m/s] | | Gurney constant [km/s] | | $V/\sqrt{2E}$ | | regarded expansion [mm] | |
|---|---|---|---|---|---|---|---|---|---|---|
| | | | point | convergent | point | convergent | point | convergent | point | convergent |
| 15813 | 29671 | 0.53 | 2327 | 2861 | 2.36 | 2.91 | 983.92 | 983.92 | 124 | 125 |
| 29476 | 29671 | 0.99 | 2305 | 2363 | 2.82 | 2.89 | 818.29 | 818.29 | 98 | 98 |
| 149501 | 29671 | 5.04 | 1087 | 1055 | 2.56 | 2.48 | 424.91 | 424.91 | 88 | 87 |
| 296127 | 29671 | 9.98 | 728 | 738. | 2.36 | 2.39 | 308.90 | 308.90 | 116 | 109 |

Table 7: Data of the Andrews configuration with PBXN-111 (core) and PBXN-110 (sleeve)

| sleeve thickness [mm] | cylinder wall velocity | disk velocity [m/s] | | | detonation velocity [m/s] | | mass of charge C [g] | | | M [g] | M/C | Gurney constant [km/s] |
|---|---|---|---|---|---|---|---|---|---|---|---|---|
| | | center | edge | ideal | sleeve | core | core | sleeve | total | | | |
| 12.9 | 1408.3 | 560 | 587 | 771.40 | 8314 | 8306 | 266 | 783 | 1049 | 2484 | 2.37 | 2.38 |
| 10 | 1324.4 | 507 | 536 | 723.09 | 8317 | 8283 | 404 | 654 | 1058 | 2484 | 2.35 | 2.23 |
| 5 | 1109.1 | 436 | 437 | 598.40 | 8310 | 8184 | 710 | 367 | 1077 | 2484 | 2.31 | 1.86 |
| 2 | 994.26 | 368 | 392 | 531.76 | 8322 | 8366 | 934 | 156 | 1090 | 2484 | 2.28 | 1.66 |

Table 8: Data of the Andrews configuration with TNT (core) and LX-14 (sleeve)

| sleeve thickness [mm] | cylinder wall velocity | disk velocity [m/s] | | | detonation velocity [m/s] | | mass of charge C [g] | | | M [g] | M/C | Gurney constant [km/s] |
|---|---|---|---|---|---|---|---|---|---|---|---|---|
| | | center | edge | ideal | sleeve | core | core | sleeve | total | | | |
| 12.9 | 1642 | 528 | 551 | 826 | 8803 | 8796 | 244 | 860 | 1104 | 2484 | 2.25 | 2.72 |
| 10 | 1576 | 494 | 511 | 798 | 8802 | 8771 | 370 | 717 | 1087 | 2484 | 2.29 | 2.63 |
| 5 | 1357 | 396 | 425 | 701 | 8806 | 8865 | 650 | 403 | 1053 | 2484 | 2.36 | 2.29 |
| 2 | 1205 | 351 | 385 | 634 | 8470 | 8963 | 855 | 172 | 1027 | 2484 | 2.42 | 2.06 |



Table 9: Energy data for the configuration with PBXN-111 (core) and PBXN-110 (sleeve)

| sleeve thickness in [mm] | explosive energy | | | $\frac{E}{TotalEnergy}$ |
|---|---|---|---|---|
| | core [kJ] | sleeve [kJ] | total [MJ] | |
| 12.9 | 807 | 4074 | 4.88 | 0.61 |
| 10 | 1226 | 3403 | 4.63 | 0.57 |
| 5 | 2154 | 1910 | 4.06 | 0.46 |
| 2 | 2833 | 812 | 3.65 | 0.41 |

Table 10: Energy data for the configuration with TNT (core) and LX-14 (sleeve)

| sleeve thickness in [mm] | explosive energy | | | $\frac{E}{totalenergy}$ |
|---|---|---|---|---|
| | core [kJ] | sleeve [kJ] | total [MJ] | |
| 12.9 | 898 | 4780 | 5.68 | 0.72 |
| 10 | 1362 | 3986 | 5.35 | 0.70 |
| 5 | 2393 | 2240 | 4.63 | 0.60 |
| 2 | 3147 | 956 | 4.10 | 0.53 |

Table 11: Data of the Andrews configuration with only one explosive

| explosive | cylinder wall velocity | disk velocity [m/s] | | | detonation velocity* [m/s] | | C [g] | M [g] | M/C | Gurney constant [km/s] | explosive energy [MJ] |
|---|---|---|---|---|---|---|---|---|---|---|---|
| | | center | edge | ideal | at cylinder wall | center | | | | | |
| PBXN-111 | 934 | 378 | 384 | 496 | 6065 | 6045 | 1100 | 2484 | 2.26 | 1.55 | 3.34 |
| PBXN-110 | 1503 | 675 | 693 | 801 | 8401 | 8275 | 1034 | 2484 | 2.40 | 2.56 | 5.38 |
| TNT | 1295 | 443 | 455 | 693 | 6772 | 6924 | 1004 | 2484 | 2.47 | 2.23 | 3.70 |
| LX-14 | 1716 | 617 | 622 | 911 | 8894 | 8786 | 1131 | 2484 | 2.20 | 2.82 | 6.29 |

* Instead of measuring the detonation velocity just along the center line of the cylinder, it was also measured directly below the cylinder wall

THIS PAGE INTENTIONALLY LEFT BLANK

# List of References


[1] S. Andrews, B. Glancy, J. Forbes, S. Collignon, and L. Hudson. Experiments on the Modification of the Energy Release Rate in a non-ideal Explosive. In *Proceedings of the conference of the American Physical Society topical group on shock compression of condensed matter*, pp. 799–802, 1995.

[2] Paul W. Cooper. *Explosives Engineering*. Wiley-VCH, Inc., 1996.

[3] Muhamed Suceska. *Test Methods for Explosives*. Springer-Verlag New York, Inc, 1995.

[4] ANSYS, Inc. *Introduction to ANSYS AUTODYN, Lecture 5, Material Models*, 2010.

[5] ANSYS, Inc. *Introduction to ANSYS AUTODYN, Lecture 2, Multi-material Euler Solver*, 2010.

[6] M. Sellam, H.N. Presles, and C. Brochet. Characterization of Strong Detonation Waves in Nitromethane. In *8th Internation Detonation Symposium*, 1985.

[7] R.W. Gurney. The Initial Velocities of Fragments from Bombs, Shell, Grenades. Technical report, Ballistic Research Laboratories, Aberdeen Proving Ground, Maryland, September 1943.

[8] J. E. Kennedy. Gurney Energy of Explosives: Estimation of the Velocity and Impulse Imparted to Driven Metal. Technical report, Sandia Laboratories, 1970.

[9] J. E. Kennedy. Explosive Output for Driving Metal. *Behavior and utilization of explosives in engineering design; and biomechanical principles applied to clinical medicine; proceedings of the 12th*, pp. 109–124, 1972.

[10] Robert A. Benham. Analysis of the Motion of a Barrel-Tamped Explosively Propelled Plate. Technical report, Sandia Laboratories, Albuquerque, NM, 1978.

[11] J.M. Short, F.H. Helm, M. Finger, and M.J. Kamlet. The Chemistry of Detonations. A Simplified Method for Predicting Explosive Performance in the Cylinder Test. *Combustion and Flame*, 43:99–109, 1981.

[12] N. Arnold, M. Estermann, and A. Koch. A Simple Relation between the Detonation Velocity of an Explosive and its Gurney Energy. *Propellants, Explosives, Pyrotechnics*, pp. 365 – 368, 2002.

[13] Jonas A. Zukas and William P. Walters, editors. *Explosive Effects and Applications*. Springer-Verlag, 2003.

[14] Mortimer J. Kamlet and S. J. Jacobs. Chemistry of Detonations I. A Simple Method for Calculating Detonation Properties of CHNO Explosives. *Journal of Chemical Physics*, 48: 23–35, 1968.

[15] D. R. Hardesty and J. E. Kennedy. Thermochemical Estimation of Explosive Energy Output. *Combustion and Flame*, 28:45–59, 1977.

[16] M.J. Kamlet and M. Finger. An Alternative Method for Calculating Gurney Velocities. *Combustion and Flame*, pp. 213–214, 1979.

[17] J. M. Short, H. G. Adolph, and M. J. Kamlet. Simplified Methods for Predicting Explosive Performance Parameters Including Eremenko's Relative Detonation Impulses. In *7th International Detonation Symposium*, 1981.

[18] E. W. LaRocca. A Simplified Method of Calculating the Gurney Constant of Common Explosives. *Presented at the 1978 Meeting Pyrotechnics and Explosives Applications Section American Defense Prepardness Association*, October 1978.

[19] B. M. Dobratz and P. C. Crawford. Properties of Chemical Explosives and Explosive Simulants. LLNL Explosives Handbook UCRL-52997 Change 2, Lawrence Livermore National Laboratory, January 1985.

[20] E. Lee, C. McMillan, N. Parker, J. Kury, C. Tarver, W. Quirk, and J. Walton. The Motion of Thin Metal Walls and the Equation of State of Detonation Products. In *8th International Detonation Symposium*, 1985.

[21] Gareth S. Collins. An Introduction to Hydrocode Modeling. http://amcg.ese.ic.ac.uk/ gsc/publications/sales_2/download/intro.pdf, August 2002.

[22] Charles E. Anderson Jr. An Overview of the Theory of Hydrocodes. *Int. J. Impact Engng*, 5: 33.59, 1987.

[23] ANSYS, Inc. *Introduction to ANSYS AUTODYN, Lecture 1, Introduction to AUTODYN*, 2010.

[24] ANSYS, Inc., Southpointe, 275 Technology Drive, Canonsburg, PA 15317. *ANSYS AUTODYN User's Manual*, release 13.0 edition, November 2012.

[25] Bryan Karosich. Blast Intensification by Detonation Merging Experimental Proof of Concept Plan and Predictions. Master's thesis, Naval Postgraduate School (NPS), June 2006.

[26] Mary Kulawiak. Strong Detonation Effects on Shaped Charges Jetting. Master's thesis, NPS, June 2004.

[27] ANSYS, Inc. *Introduction to ANSYS AUTODYN, Lecture 4, AUTODYN Basics*, 2010.

# INITIAL DISTRIBUTION LIST

1. Defense Technical Information Center
   Ft. Belvoir, Virginia

2. Dudley Knox Library
   Naval Postgraduate School
   Monterey, California

3. Research Sponsored Programs Office, Code 41
   Naval Postgraduate School
   Monterey, CA 93943